Beam emittance measurements in the SPC2 injection beamline at iThemba LABS

A thesis submitted in accordance with the requirements for the Masters degree in Physics in the Department of Physics and Engineering, University of Zululand

By Ndumiso Mnikathi

Supervisor: Prof. S.S. Ntshangase (University of Zululand)
Co-Supervisor: Dr. F. Nemulodi (iThemba LABS)

June, 2021

Declaration

I, the undersigned, hereby declare that the work contained in this thesis is my own original work and that I have not previously in its entirety or in part submitted it at any university for a degree.

Signature Date

Abstract

Beam emittance is a property of a charged particle beam in a particle accelerator that is used to estimate the beam quality. It is length-based measure of the average spread of particle coordinates in position and momentum phase space. This attribute makes emittance a crucial beam parameter that one requires when tuning the beam into smaller spaces in a beamline and matching the beam with the acceptance of an accelerator. At iThemba LABS, the low energy beam transport (LEBT) system required a system that measures transverse beam emittance. This beamline connects the two electron cyclotron resonance ion sources (ECRIS) to the second solid pole injector cyclotron (SPC2) and is composed of a set of solenoid and quadrupole magnets that are used to focus the beam. This layout makes it possible to use solenoid and quadrupole magnets to carry out beam emittance measurements.

This thesis is aimed at presenting a developed system that can be utilized for measuring transverse beam emittance of beams emerging from the ECRIS. An analytic explanation of the techniques used and tools needed for these measurements are given. The Gauss approximation program and the emittance calculator were developed and used. During the development process, the system was validated using different beams simulated using a computer program TRANSPORT [1]. The beam widths obtained from TRANSPORT were used on the developed emittance calculator to establish if one could get the injected beam emittances. From the calculations it was clear that there is an agreement between injected and deduced emittances. This was an indication that the emittance calculator is working as expected. Thenceforth, the real beam emittance measurements were performed using $^{4}He^{2+}$ beam with kinetic energy $E_k = 12.7$ keV. After analysing the helium data it was decided that a second set of measurements should be performed and this was done using $^{32}Si^{5+}$ beam with kinetic energy $E_k = 8.35$ keV.

The obtained results from both helium and silicon measurements were analyzed in order to compare the emittance measured in the AX-line with the one measured in the Q-line. From both set of measurements it was observed that the emittances obtained in the two beamlines had some disagreement. This disagreement between the two sets of transverse emittances violated Lioville's theorem. In order to probe the source of disagreement the helium measurements were further investigated by performing beam widths comparison. To do this, the measured emittances were injected into TRANSPORT and the beam widths gathered were then compared with the measured widths. From the comparison results it was clear that only the beam widths from AX-line are comparable while there was disagreement in Q-line widths comparison. It was evident from these observations that one could

rely on beam emittances obtained in the AX-line than those obtained from Q-line beamline. Upon further investigation, it was concluded that reason behind this could be associated with the fact that for AX-line measurements, instead of performing minimum number of measurements (i.e three) required to deduce the emittances, five set of measurements were utilized instead. This choice of number of measurements makes the system robust in such a way that a small error on measured beam widths will have a negligible effect on the deduced emittances. For Q-line measurements, however, the solenoids scan was performed with minimum number of beam widths measurements (i.e ten) required. This may have resulted in the solenoid scan being sensitive to errors that could occur when measuring beam widths. For much more reliable emittance measurements in the Q-line the system needs to be upgraded in order to accommodate utilization of more beam widths of measurements.

Acknowledgements

Firstly I would like to express my gratitude to my supervisors Dr. Fhumulani Nemulodi and Prof. Sifiso Ntshangase. Thank you for your guidance and support throughout my research journey I am forever grateful. To Dr. Nemulodi thank you, for your patience, understanding and providing me with every tool that I needed in order to make my research a success. Your coding enthusiasm is contagious and I have learnt a lot from you. To Prof. Ntshangase your academic and financial support was amazing thank you. I would like to also thank the following people:

- Dr. Joele Mira for welcoming me in the accelerator department even though our initial project did not work out. Whenever I had a question your door was always open.
- Dr. Muneer Sakieldien for your financial support and the good energy that you have.
- Dr Rainer Thomae for opening your door for queries I had. You made physics a little bit easier to grasp with your explanations and drawings

Ngiphinde ngithathe ithuba lokubonga abazali bami ngokungipha impilo, ukungithemba, kanye nokungiseka ngokomphefumulo. Ngiyazi anikutholanga lula ukwamukela ukuthi ngihlale kude nani. Kumfowethu nakodadewethu ngithi *"if I can do it, they can also do it"*. I would like to dedicate this work to my dad.

Last but not least I would like to thank the National Research Foundation (NRF) for financial support. iThemba LABS for providing me with all necessary infrastructure to complete this study.

Contents

List of Figures

List of Tables

Acronyms

iThemba LABS iThemba Laboratory for Accelerator Based Sciences

SPC1 Solid Pole Cyclotron 1

SPC2 Solid Pole Cyclotron 2

SPI Source for Polarized Ions

OPAL Object Oriented Parallel Library

RF Radio-Frequency

PIG Penning Ionization Gauge

EPICS Experimental Physics and Industrial Control System

ECRIS Electron Cyclotron Resonance Ion Source

DC Direct Current

RMS Root Mean Square

GUI Graphical User Interface

LEBT Low Energy Beam Transport

SSC Separated Sector Cyclotron

HMI Hahn Meitner Institute

GTS Grenoble Test Source

OPERA-3D OPerating environment for Electromagnetic Research and Analysis

EEC Electrostatic Extraction Channel

MEC1 Magnetic Extraction Channel 1

MEC2 Magnetic Extraction Channel 2

GANIL Grand Accélérateur National d'Ions Lourds

Chapter 1

Introduction

A beam of particles can be characterized in detail by its density in the six dimensional phase space $(x, x^{'}, y, y^{'}, z, p_z)$ where $x^{'} = \frac{dx}{dz} = \frac{p_x}{p_z}$ and $y^{'} = \frac{dy}{dz} = \frac{p_y}{p_z}$. Positional coordinates x and y respectively describe the horizontal and vertical displacement of the arbitrary ray with respect to the assumed central trajectory. The $x^{'}$ and $y^{'}$ slopes respectively describe the angle the ray makes in the horizontal and vertical planes with respect to the assumed central trajectory. These angles are respectively derived from their related momenta p_x and p_y. Lastly, z is the path length difference between the arbitrary ray and the central trajectory and p_z is the fractional momentum deviation of the ray from the assumed central trajectory [1]. Positions x and y describe the transverse direction and z describes the longitudinal direction as shown figure 1.1.

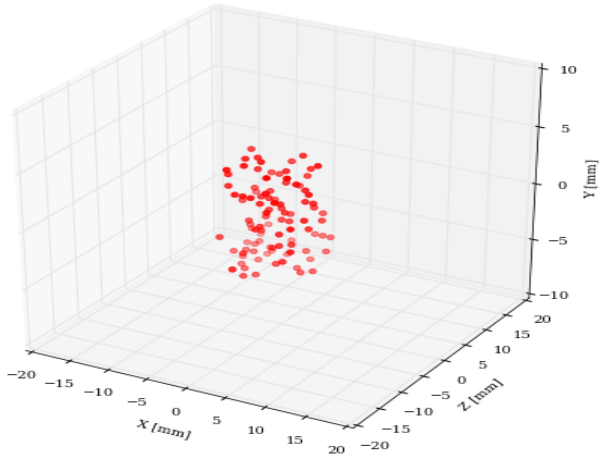

Figure 1.1: An illustration of a beam of particles in 3-dimensional space coordinates x, y and z.

Shown in figure 1.1 is an illustration of beam of particles in three-dimensional space. Each particle is represented by its three directional coordinates x, y, and z. As explained above each particle has an additional coordinate related to their momentum, i.e. p_x, p_z and p_z. This use of this six-dimensional phase space to describe particle density is derived from Sturm Liouville's theorem which involves the use of constant conservative fields [2] to act on the particles. For any beam of charged particle, the six dimensional phase space can be split into three, two-dimensional subspaces (x, x'), (y, y') and (z, p_z) [3]. The subspaces (x, x') and (y, y') are used to describe the transverse beam properties whereas for longitudinal beam properties (z, p_z) subspace is used. Figure 1.2 shows the distribution of particles in (x, x') phase space. The same distribution can also be illustrated in the other two phase space subspaces, i.e. (y, y') and (z, p'_z).

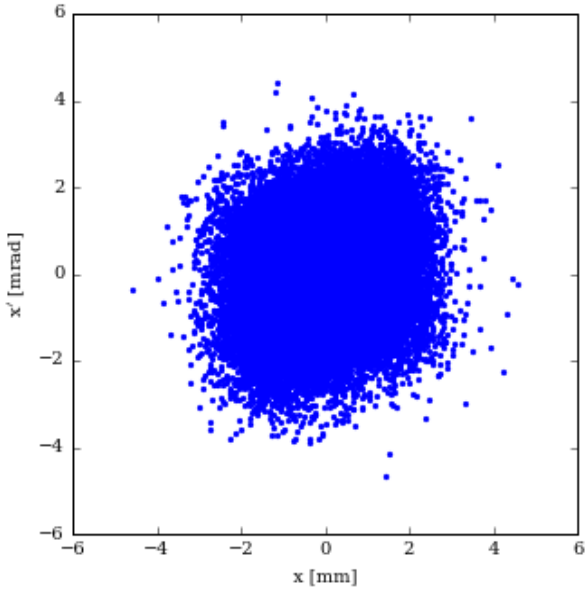

Figure 1.2: A distribution of beam of particles in (x, x') phase space.

Traditionally, the beam of charged particles are generated using ion sources through plasma generation. These beams emerging from these ion sources have an attribute known as emittance (ε) which is measured in π mm mrad[§§]. Emittance is a trait of the particle beams that characterizes its size [4]. It defines an area or volume in the phase space of particles. Emittance plays a vital role as it can be used to

[§§]Often a π is added to the unit of emittance to indicate that the numerical value describes a surface in (x, x') space divided by π. This unit will be adopted in this work.

infer the quality of the beam. It can be used to evaluate the ability of the beam to be transported over long distances and be focused into small space with minimum divergence as well as the capability to form high resolution images. In the current study, only transverse beam emittances are considered i.e ε_x and ε_y.

There are number of techniques that can be employed in an attempt to measure transverse beam emittance [5]. In the current study only two methods are employed, namely; quadrupole scan and solenoid scan. The quadrupole scan technique which is also known as "three gradients" method [6] is one of the well understood method of measuring transverse beam emittance. The principle for this technique entails the alteration of the quadrupole's magnetic field strength at least three times. At each magnetic field strength, the horizontal and vertical beam widths are measured using the profile monitors. The obtained beam widths along with their corresponding magnetic field strengths are then used to compute transverse beam emittance.

As already mentioned, the "three gradients" method involves the use of quadrupoles. However, in the SPC2 low energy beam transport (LEBT) beamline quadrupoles are only situated in the second segment of the beamline, with first part of the beamline only utilizing the solenoid magnets. The project in hand is centered around obtaining the transverse emittance of beams emerging from the electron cyclotron resonance ion sources (ECRIS). In order to be able to deduce the emittance from the ECRIS the beam emittance measuring system being developed should be able to perform measurement at a position in vicinity of the ion sources. Hence, the additional method that utilizes the solenoids lenses to calculate emittance was developed. The working principle for this method is similar to that of quadrupole scan with the only difference being that the solenoid's magnetic field strength is altered at least ten times instead of three times. This is due to the fact that solenoid magnet introduces the coupling between the two transverse directions which results in the two directions not being able to be treated independently (see chapter 3 for more details). In keeping the same naming convention, this technique is named the "ten gradients" method. The details of how both "three" and "ten" gradients methods are derived are explained in chapter 3.

Motivation for the study

iThemba LABS (Laboratory for Accelerator Based Science) has a second solid-pole injector cyclotron (SPC2) that has three external ion sources, the two ECRIS and the ion source for polarized ions (SPI). These sources are located in the basement below the (SPC2) vault. In this work only the beamline from ECRIS is of interest. The ECRIS are used for generation of both light and heavy ions which are then transported using LEBT before injection into SPC2 for pre-acceleration. The LEBT is composed of solenoids, quadrupoles, bending magnets and steering magnets. Also available are the diagnostic tools used for measuring beam current as well as beam profile. Beam current is measured using faraday cups and beam profile is monitored using multi wire scanners (harps).

Currently, SPC2 has an overall transmission of approximately 10% for heavy ions. This transmission is not adequate for delivering high-intensity high-energy beams. In order to improve the transmission several ideas are currently being investigated through simulation studies. Some of these studies are briefly discussed below;

- The effect of the additional buncher on the vertical beamline of the LEBT was studied using Object Oriented Parallel Library (OPAL) code.
- A new spiral inflector was modelled using TOSCA.
- Electric and magnetic fields of SPC2 modelled in 3 dimension (3D) using OPERA-3D [7, 8].

The bunching efficiency of the second buncher operating at the second harmonic was investigated in the vertical beamline using OPAL code[9]. Through simulations, the beam dynamics were studied to investigate how the addition of the buncher operating in second harmonic mode would affect the beam transmission through SPC2 cyclotron.

Another investigations were performed on how the spiral inflectors could be improved. Here, the spiral inflector C (see section 2.3 for infelctors naming convention) which bends the axially injected beams into the median plane of SPC2 were investigated. These C inflectors

are mainly used for heavy ions and "C inflector" is just a naming convention. C1 inflector is an old version and C2 inflector is a new modelled version. They are both based on Belmont-Pabot [10] designs. Which means they have a good transmission, but suffer from vertical defocusing [11]. Therefore the study involving, shaping the inflector electrodes such that they create a quadrupole electric field along the path length, in order to create a strong focusing effect was done. The simulation package TOSCA was used to model the beam passing through the C2-inflector of Solid Pole Cyclotron 2 (SPC2).

In performing the above mentioned simulation studies, the knowledge of the emittance from the ion sources is required, as this is an important parameter injected into the simulation codes. At present there is no system in use that measures beam emittance in the low energy beamline at iThemba LABS. Such system is only available in the high energy beamline whereby the multiple monitors method is used to determine beam emittance. Due to this reason simulations are being performed with estimated emittance values. This estimation of emittance might result in undesirable conclusions. It is the aim of this work to mitigate such problem.

The main objective of the project at hand is to develop a method that will help users to easily measure the transverse beam emittance in the beamline from the ECRIS to SPC2. This measure can be used as an input parameter for beam simulation codes. And with the knowledge of beam emittance it is anticipated that the reliability of simulation results can be improved. Also, knowing the emittance from the ion sources will help users to tune the beam such that it matches the acceptance of SPC2. This can also improve the transmission through SPC2.

Outline of Thesis

The thesis is structured as follows:

- In chapter 2 the iThemba LABS accelerator facilities are described briefly.
- Beam dynamics and parameters that are considered and required

for beam emittance calculations are presented in detail in chapter 3.

- The experimental conditions, equipment and setup are presented in chapter 4.
- The measurement results and discussion are presented in chapter 5.
- Finally, conclusions and outlook derived from this study are presented in chapter 6.

Chapter 2

Layout of the Facility

iThemba LABS is a multidisciplinary research facility, operated by the National Research Foundation (NRF) of South Africa. It provides accelerator facilities for research and training in the physical, biomedical, material sciences as well as production of radioisotope and radiopharmaceuticals for use in nuclear medicine and industry [12]. At the heart of iThemba LABS, is a separated sector cyclotron (SSC) which is used for final acceleration of charged particles to higher energies. The two solid-pole injector cyclotrons, SPC1 and SPC2 are used to pre-accelerate the charged particles. Shown in figure 2.1 is the current layout of the cyclotron facility with different beamlines. The working principles of the cyclotrons are discussed in this chapter along with the beamline of interest and its ion sources.

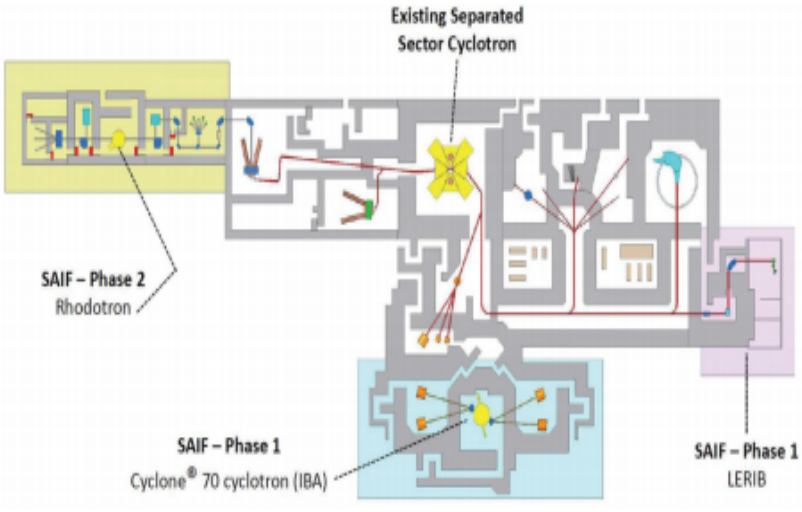

Figure 2.1: The existing layout of the Separated Sector Cyclotron facility of iThemba LABS. Also shown are the shaded areas which are the planned facilities for the future [14].

2.1 Cyclotron Accelerators

The fundamental working principle for cyclotrons with two 180^0 D-electrodes is illustrated in figure 2.2 and can be summarized as follows: A beam of particles is accelerated in a gap between two electrodes usually referred to as dees (D's) when there is a potential difference between them. The dees are connected to an RF generator and are placed in a uniform magnetic field [13]. The beam injected at the centre of the cyclotron is attracted to the dee with the opposite polarity as that of the beam. The vertical magnetic field causes the beam to bend into semi-circles inside the dee and across the gap between them. As the beam is following a semi-circular path the polarity of the electrode changes. When it reaches the gap, the electric field accelerates them further. This process happens continuously and the beam gains more and more kinetic energy as it orbit the semi-circles. The radius of the beam path increases in proportion to $r = \frac{mv}{BQ}$*, as the beam travels faster. The radius of its path increases and so despite travelling faster, it takes the same time to travel each semi-circle, so the alternating voltage is operated at the same frequency.

Cyclotrons are often named using a K-value in [MeV] as a prefix [15]. The K-value of the cyclotron indicate the cyclotron's performing index that gives the maximum energy that it can attain for protons. The K-value of a cyclotron is given by:

$$K = 47.89(B\rho_{em})^2 \tag{2.1}$$

where $B\rho_{em}$ is the protons rigidity at extraction.

2.1.1 The First Solid Pole Injector Cyclotron (SPC1)

A $K = 8$ SPC1 injector cyclotron (shown in figure 2.3) is used for pre-acceleration of light ion beams. This injector cyclotron is equipped with an internal Penning Ionization Gauge (PIG) ion source which is used for generation of the light ions. This cyclotron is a four-sector machine with two 90^0 dees which can attain a maximum dee voltage of 60 kV. It is operated with either 2^{nd} or 6^{th} harmonic mode. The RF-system for this injector has a frequency tuning range from 8.6 MHz to

*where m, v, Q and B respectively denote mass, velocity, charge state of the particle and magnetic field of the cyclotron

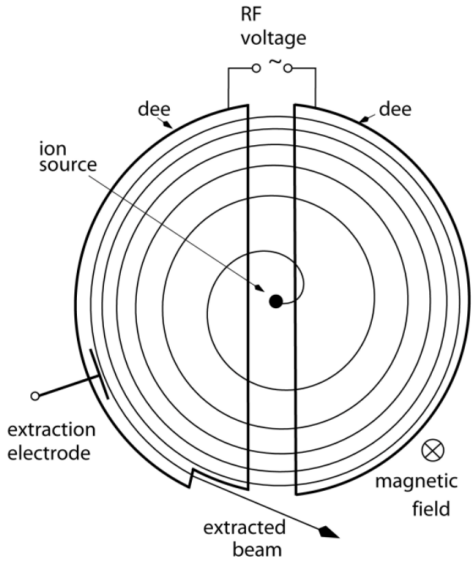

Figure 2.2: The illustration of the working principle of the cyclotron with two 180^0 D-electrodes[15].

26 MHz which is achieved by utilizing the movable short-circuit plates in the quarter-wave transmission lines. The maximum flux density attainable for this machine is 0.86 T. The cyclotron has an extraction radius of 0.476 m and the beam is extracted by using an Electrostatic Extraction Channel (EEC) and the two Magnetic Extraction Channels, MEC1 and MEC2 [16, 17]. In most cases this cyclotron is used to pre-accelerate protons which are used for radioisotopes production.

2.1.2 The Second Solid Pole Injector Cyclotron (SPC2)

The K=11 SPC2 (shown in figure 2.4) is used for pre-acceleration of both light and heavy ions as well as polarized proton beams. Just like SPC1, it is a four-sector cyclotron with two 90^0 dees which can also attain a maximum dee voltage of 60 kV. The 2^{nd} and 6^{th} harmonic modes are used for acceleration. The RF-system has a frequency tuning that ranges from 8.6 MHz to 26 MHz with movable short-circuit plates in quarter-wave transmission lines. The maximum magnetic flux density of operation is $\sim$1 T with an extraction radius of 0.476 m. The extraction of the beam is also achieved by utilizing the EEC as well as the two magnetic channels. Unlike the SPC1, SPC2 is fed by the three ion sources which are situated in the basement. Beams

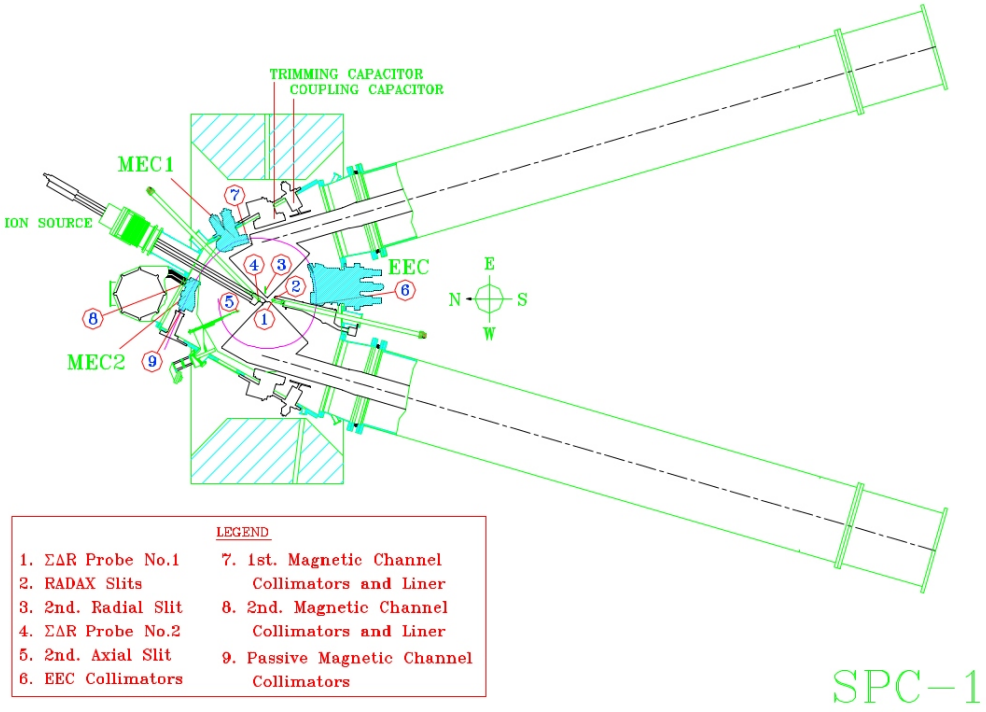

Figure 2.3: A cross-sectional drawing of the SPC1 for light ion acceleration.

from these sources are axially injected into SPC2 using the three interchangeable spiral inflectors. These three different inflectors are used in order to achieve three orbit geometries [18]. Depending on the final energy required and ion species to be accelerated, ions can make 8, 16, or 32 turns before extraction [9].

2.1.3 The Separated Sector Cyclotron (SSC)

As already mentioned, the final acceleration of ion beams to higher energies is achieved by using the SSC accelerator. The schematic diagram of the SSC is shown in figure 2.5. The SSC is a $K = 200$ cyclotron which has four separated sector magnets with a sector angle of 34^0 and overall diameter of 13 m. The height of the cyclotron is 7 m. The vacuum chambers of the machine are mounted in the pole gaps and between the magnet sectors. The maximum flux density in each sector is 1.256 T in the 66 mm pole gap. Using the $\frac{\lambda}{2}$ resonators by means of short plates and variable capacitors the RF-system can be tuned from 6 to 26 MHz [19, 20]. The dees with an angle of 49^0 can be operated up to a maximum voltage of 250 kV. The 4^{th} and 12^{th} harmonic modes are used for acceleration. The extraction of the

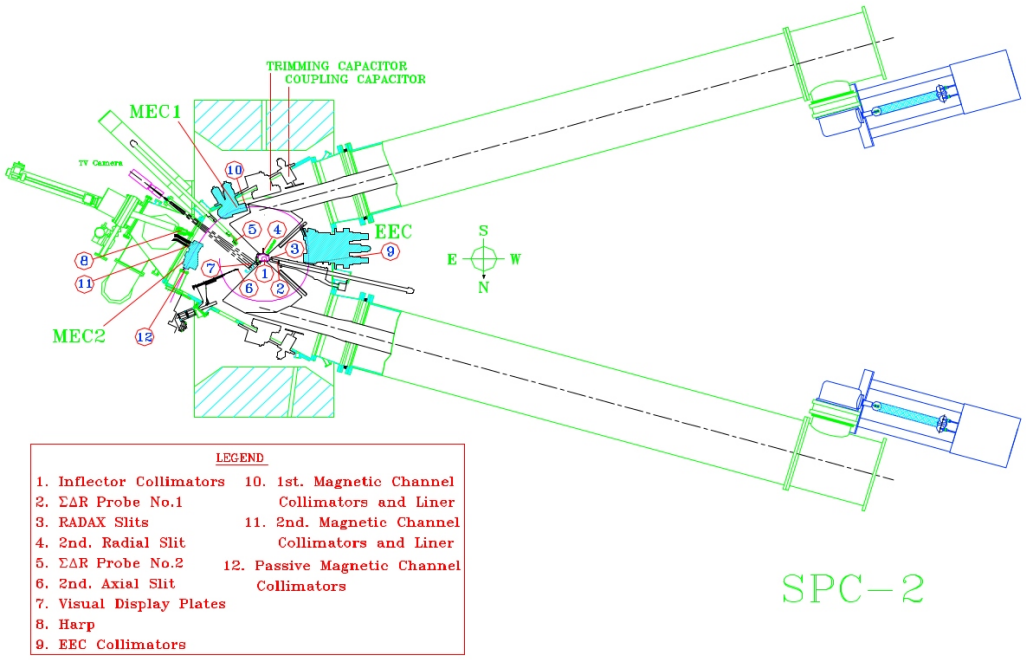

Figure 2.4: A cross-sectional drawing of the SPC2 for light, heavy and polarized ion acceleration.

beams is achieved by using two septum magnets.

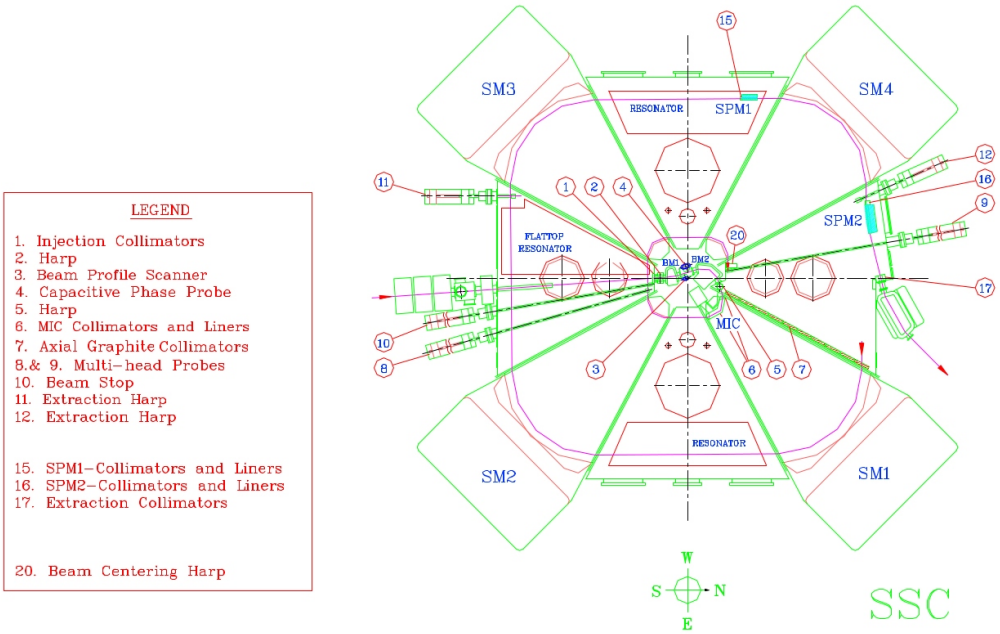

Figure 2.5: A cross-sectional drawing of the SSC at iThemba LABS.

2.2 The ECR ion sources at iThemba LABS

The ECRIS are types of sources which are widely used for the production of high quality singly and multiply charged ion beams [21]. The working principle of ECRIS is that it has a cylindrical chamber which contains plasma that is confined by the magnetic field. There are several configurations in ECRIS but in this case our focus is the type of ECRIS with the design similar to the one shown in figure 2.6. This design is aimed at achieving the production of highly charged ion beams. The magnetic field is generated by a combination of solenoidal coils and permanent magnets. The coils generate a magnetic mirror field which provides axial confinement of the plasma making electron bounce back and forth axially. The strength increases axially providing axial confinement and it is weaker radially, not providing confinement. To provide radial confinement a second magnetic field configuration is added. The radial field is generated using permanent magnets which produce a hexapole field. Adding this field to the mirror field causes the field lines to bend outwards towards the chamber wall [22, 23]. The confined electrons are heated by electron cyclotron resonance with an external RF power source and ions are generated through impact ionization with the heated electrons. Then the ion beams are extracted from the source's plasma chamber.

Generally, there are two types of extraction systems that are commonly used for extracting charged particles from the ion sources namely; the diode system and the triode system. In the diode system, two electrodes are used to accelerate and guide the ion beams out of the source. The first electrode is called the plasma electrode and is also commonly known as extraction electrode. It is in contact with the plasma inside the source and operates on ion source potential. It also has an extraction aperture which allows the ion beams to exit the source. The second electrode is called a ground electrode and it is fixed at ground potential. Thus, the ion accelerating electric field is between the electrodes. The distance between the two electrode is called the extraction gap. The triode system is similar to the diode system but has one extra electrode which is placed between extraction electrode and ground electrode. This additional electrode is known as a suppressor electrode. It is held at a negative potential, so that it

repels stream of electrons back into the ion source from downstream. This system is also is also known as accel-deccel triode system [24]. In the following sub-section the ECRIS at iThemba LABS will be briefly discussed.

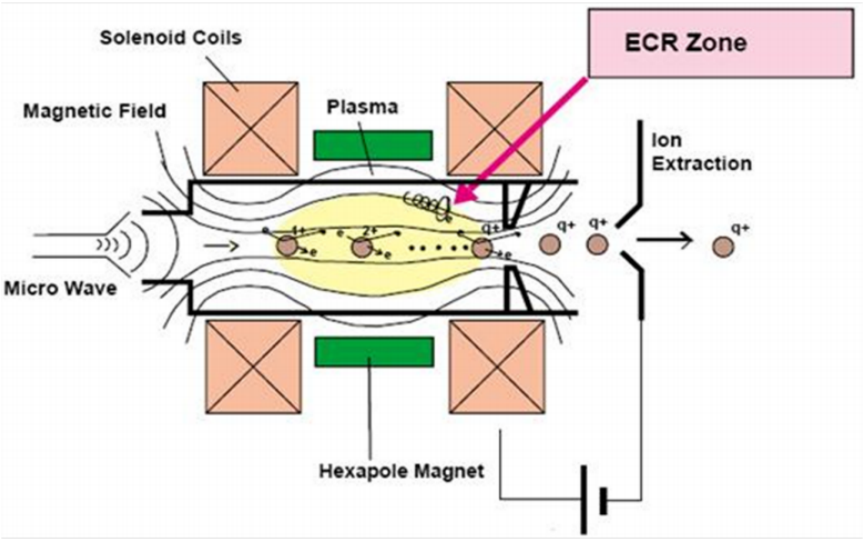

Figure 2.6: The layout of an ECRIS showing the important parts used to achieve highly charged ions [25].

2.2.1 HMI-ECR Ion Source

The HMI-ECRIS was donated to iThemba LABS by Hahn Meitner Institute (HMI) [26] and has been in operation since 2008 [27]. The source was originally built by Grand Accélérateur National d'lons Lourds (GANIL) for HMI. It is a modern room temperature type of ECRIS. It serves to provide highly charged heavy ions which are used for nuclear physics research. The source is linked up with the beam-line leading to SPC2. It is made up of a water-cooled plasma chamber with the length of 18 cm and the diameter of 7 cm. The chamber is surrounded by FeNdB permanent magnets which produce a hexapole field of 1 T for radial plasma confinement. For axial confinement of the plasma two solenoid coils are used. The field on the axis can be altered from 0.4 to 1.1 T. The source is also equipped with a 14.5 GHz RF generator that can deliver a microwave power of up to 2 kW [28]. The microwave power is injected into the source chamber through a wave guide. In order to produce different ion species, the ion source

has a flexible design such that it can operate with an oven and sputter target techniques. The ion beam is extracted using the diode system. The plasma electrode has an aperture of 8 mm in diameter and its potential can be altered between 2 and 20 kV. The ground electrode has aperture of 13 mm and the extraction gap is 20 mm [17]. Shown in figure 2.7 are the two ECRIS situated in the basement below SPC2 vault.

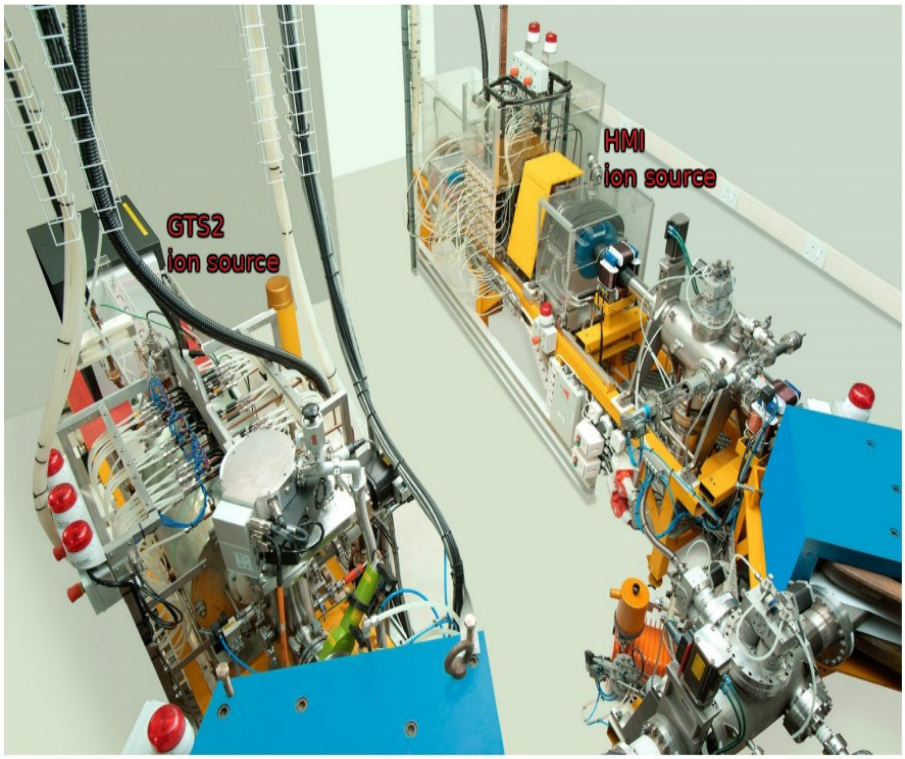

Figure 2.7: The picture of the two ECR ion sources at iThemba LABS.

2.2.2 GTS-ECR Ion Source

Just like the HMI-ECRIS the GTS-ECRIS is also a modern room temperature ECRIS and has been in operation since 2009. This source has a double wall plasma chamber with an axial length of 30 cm and a diameter of 8 cm. This plasma chamber is made up of aluminium and it is surrounded by permanent hexapole magnets which are made of FeNdB material. The hexapole is arranged in the Halbach structure and has a radial magnetic field strength of 1.3 T for radial plasma confinement. Three sets of coils are used to produce axial magnetic field, with the centre coil used for tuning the minimum magnetic field

for axial confinement of plasma. The axial magnetic field can be altered from 0.5 T to 1.2 T using copper coils powered by large current supplies. The ECRIS is coupled with 14 and 18 GHz microwave generators through water-cooled waveguides. This gives the source the flexibility to be operated in either a single or double frequency mode. The particle beams are extracted using a diode system. The plasma electrode has an aperture of 9 mm in diameter and its potential can be varied between 2 and 20 kV. The ground electrode has an aperture of 12 mm in diameter and the extraction gap is 40 mm. In addition, the source design includes two ovens of which they can be used to produce metallic vapours for ion beam production [17].

2.2.3 psedo Beam Generation with GTS Ion Source at iThemba LABS

In order to be able to generate a beam of charged particles several source parameters need to be set to optimal values. Suppose one needs to generate a beam of argon particles with $^{40}\mathrm{Ar}^{8+}$ being charge state of choice. The ^{40}Ar gas would be injected into the source's discharge chamber which operates in vacuum. The vacuum's low pressure must be between 10^{-4} - 10^{-3} Pa and this is achieved by using forepumps and turbo molecular vacuum pumps. A 14 GHz microwave generator is used to produce microwaves. These microwaves are injected into discharge chamber where the ^{40}Ar gas is, so that ionization is triggered. In the process of ionization the injected microwaves will excite the electrons of ^{40}Ar gas then the excited electrons would then strip away from the atom leaving it ionized. This process is done under the influence of magnetic fields from solenoid magnets and permanent magnets so that the plasma would be confined.

The plasma is confined both axially and radially. Radially the plasma is confined by FeNdB permanent magnets with the magnetic field of 1.3 T and axially three solenoid coils with a magnetic field which may vary from 0.5 T to 1.2 T. The current in the middle coil is opposed to the other two coils to create the dip in the overall magnetic field strength.

Ion confinement also plays a critical role whereby if ^{40}Ar ions confinement time is too short ions won't reach high charge state (8^{+}) and

if its too long the high charge state ions decay by charge exchange. Therefore, the source must be operated at optimum. Also the plasma electrons must be in the temperature around 1 keV and 10 keV which is good for producing the highly charged ions like Ar^{8+}. The $^{40}Ar^{8+}$ beam would be extracted using the diode system. The ions are extracted and accelerated towards a grounded extraction electrode by applying a high voltage of typically 12.4 kV to the discharge chamber. Shown in figure 2.8 is the source monitor displaying a stable beam current.

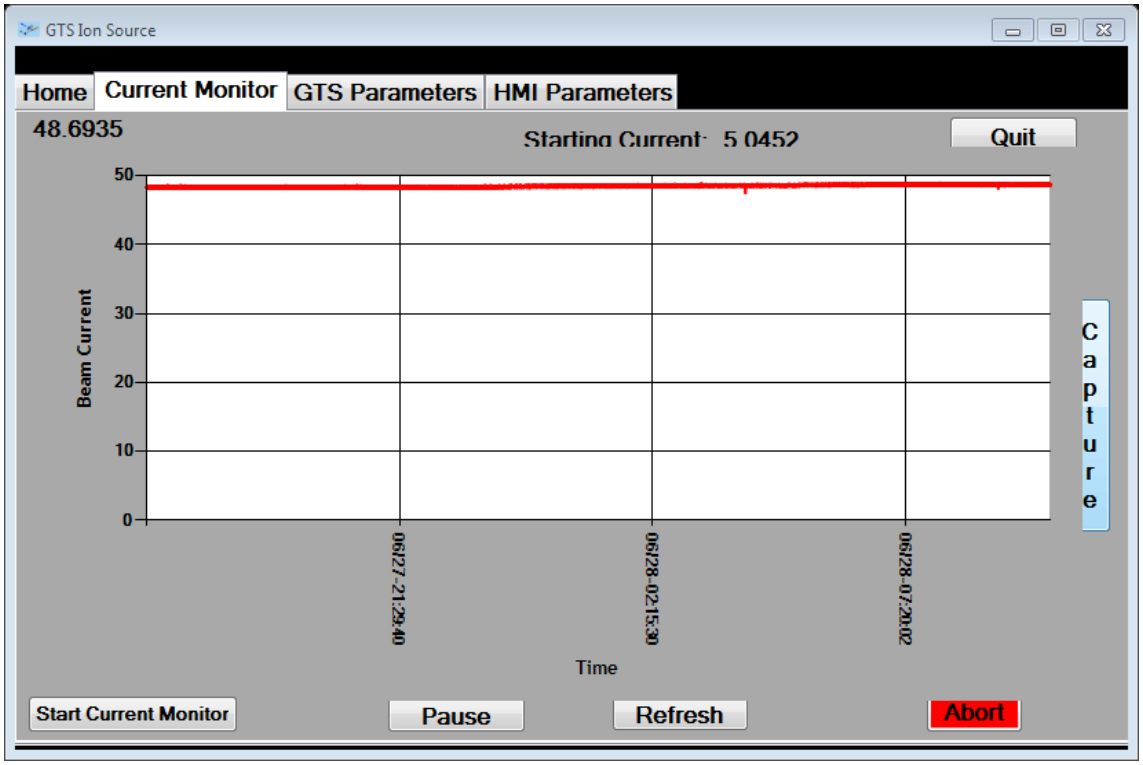

Figure 2.8: Beam current monitor that shows the stability of the beam extracted.

2.3 Injection Beamlines leading to SPC2

As already mentioned, the two ECR ion sources are located in the basement below the SPC2 vault. Figure 2.9 shows the complete schematic view of the LEBT from the two ECR ion sources leading to the SPC2 cyclotron. The charged particle beams extracted from these sources are transferred through a beamline divided into two segments namely; the Q-line and vertically aligned AX-line. The Q-line consists of the two bending magnets B1Q and B2Q, solenoid magnets (L2Q-L5Q, R1

and R2) and the two harps (harp 3Q and 5Q). The beam extracted from the GTS source is bent into the horizontal Q-line with a 104^0 B1Q magnet. This bending magnet is also used as a mass analyser to separate different charge states of ions. The solenoids (L2Q-L5Q) are identical, so are the rotatable solenoids R1 and R2. The solenoid magnets are used for focusing the beam in the first segment of the LEBT. The two harps 3Q and 5Q are used for beam profile monitoring while Faraday cups are also available for measuring beam current. The beam is bent into the vertical beamline through the bending magnet B2Q.

The AX-line consists of six quadrupole magnets (Q1-Q6), harp 1AX and harp 2AX, a buncher and the two solenoid magnets L1AX and L2AX. The quadrupoles are used to focus the beam to a double waist at the entrance of the buncher. They are arranged as a two-triplets with Q1 and Q3 connected in series [28]. The harps 1AX and 2AX are used for beam profile monitoring, the buncher is used for grouping charged particles into bunches. And the two solenoids L1AX and L2AX are used to focus the beam just before it is axially injected into the cyclotron. The marked points P1 and P2 shown in figure 2.9, are the points where the transverse beam emittance will be measured.

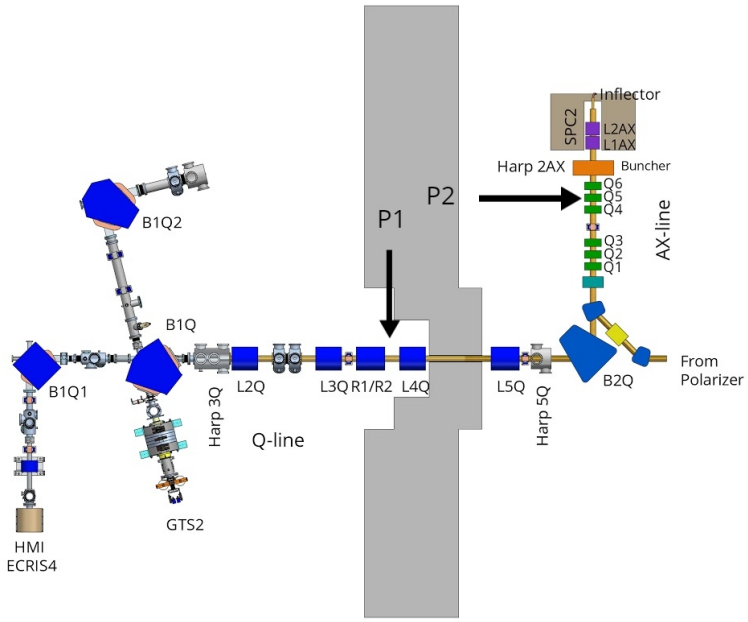

Figure 2.9: The low energy beamline transport leading to SPC2. Also shown are the two schematic view of the ECRIS.

A buncher is a device that groups charged particle beams into bunches

such that the number of particles that can be accelerated by cyclotron can be increased. They are normally used to increase efficiency of particle accelerators with external ion source(s). The direct current (DC) beam from the external ion source is pulsed by the buncher so that the period of the pulsed beam is matched to RF frequency of the cyclotron [29]. There are different ways in which the bunching process is achieved and in this case, bunching by velocity modulation using radio frequency (rf) cavities is used in the injection beamline. The beam is bunched by introducing velocity modulation with an rf cavity over a distance [30]. The front beam is decreased while at the back its increased by using rf staggering. Shown in figure 2.10 is a double gap buncher which operate in 1^{st} harmonic in the AX-line.

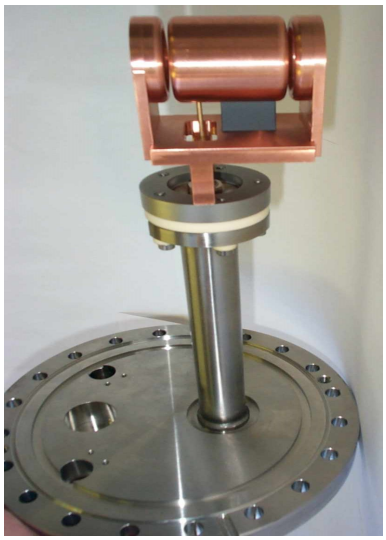

Figure 2.10: A picture of a buncher currently in used in the LEBT at iThemba LABS.

Spiral inflectors are electrostatic electrodes that are twisted like a spiral such that they bend the beam 90^0 into the median plane of the cyclotron. In this case the AX line is vertically connected to SPC2 which makes them perpendicular to one another. The charged particle beams from external ion sources must be bent 90^0 in order to be accelerated by the cyclotron. The spiral inflector is used to achieve this. The beams are axially injected into the cyclotron for acceleration and the electric fields on the electrodes of the spiral inflector are orthogonal to the beam as the beam gets bent by the cyclotron's magnetic field [31]. There are different designs for inflectors and shown in figure 2.11 is a design based on Belmot and Pabot [10].

Belmot and Pabot are the inventors of the first spiral inflector, and their design is based in consideration of the following conditions [10].

- The first orbit of the injected charged particle beams to be accelerated by a cyclotron should coincide with a set out position.
- The axial motion of charged particle beams must be transformed into horizontal orbital motion inside the cyclotron accurately.
- As the orbital radius increases when charged particle beams get accelerated, the first turn must be greater than half the horizontal dimension of the deflector gap plus the distance between the deflector and the dummy dee.

Such design is known to have a good transmission, but suffer from vertical defocussing, which can lead to beam loss in the inner region of the cyclotron. The C2 and C3 inflectors shown in figure 2.11 are newly improved version which have improved vertical focusing (see [11]) in order to improve the transmission of heavy ions[†].

Figure 2.11: This picture shows the newly designed spiral inflectors that are used for 8 turns patterns in the SPC2 injector cyclotron.

[†]SPC2 cyclotron at iThemba LABS has three turns patterns. Each pattern requires its own inflector, these inflectors are named A (32 turns), B (16 turns) and C (8 turns)

2.4 Considerations During the Initial Beamline Design

Initially, the injection beamline was designed for the ECRIS which was located 180^0 anti-clockwise to where HMI ECRIS is located (see [28] for more details). In order for the dispersion path to lie in the bend plane of each dipole, the beam extracted from this source needed to be rotated by exactly 90^0 between the two dipole magnets. Several focusing elements were considered for the horizontal section between the two bending magnets. After investigation it was concluded that solenoid magnets are best focusing elements to use as they could form a natural achromat. This desired achromat is formed as a mirror symmetric system between two 90^0 dipoles [32]. The beamline between the dipole magnets can be classified as a two identical sections. Section one composed of solenoids L2Q, L3Q and section two composed of solenoids L4Q and L5Q. For solenoids L2Q and L3Q, the first-order transfer matrix is the identity matrix -I, with no rotation of the beam. In the second half of the system, the solenoids are powered very similar, however this time with similar polarity. The first-order transfer matrix is again -I, however, the beam is rotated 90^0. The total transfer matrix is then +I, with 90^0 rotation as required [28]. The rotatable solenoids R1 and R2 are operated with opposite polarities and they lie on the symmetry plane. The results obtained in this work can also be used to verify if these initial considerations are still achievable with the use of the 104^0 bending magnet that is currently being utilized for GTS ion source instead of the 90^0 bending magnet that beamline was designed with.

Chapter 3

Beam Dynamics & Parameters

In this chapter basic concepts of beam dynamics related to the current study are discussed. The mathematical formalism for particle beams going through different segments in the beamline is also introduced. Different magnetic elements are also introduced. Liouville's theorem involving Hamiltonian is briefly discussed. Finally, the parameters and concepts required for emittance measurements are also discussed.

3.1 Transfer Matrix formalism

There are different methods that can be employed to model the beam of particles traversing through different elements in the beamline. Such methods include the use of Monte Carlo simulation which employs the tracking of particles as well as the use of matrix formalism to calculate particle trajectories. The modelling of particle beams in the beamline by calculating particle trajectories can be done by using the transfer matrix formalism. This describes the effect of ion optical elements (and drifts space between them) on trajectories using transfer matrices. One can use a vector $\mathbf{X}$, which its density in phase space can be characterized in 6D as shown in Chapter 1,

$$\mathbf{X} = \begin{vmatrix} x \\ x' \\ y \\ y' \\ z \\ p_z \end{vmatrix}. \tag{3.1}$$

A system that describes the particle represented by the above vector passing through a lens can be represented by the matrix. For an example a quadrupole magnet which can be represented by the first order square matrix R (R is a matrix that describes the action of the magnet on the particle coordinates see [33]) can be resolved into a matrix multiplication as follows [1]

$$\mathbf{X}(1) = R\mathbf{X}(0) \ . \tag{3.2}$$

The vector $\mathbf{X(0)}$ is the initial coordinate and $\mathbf{X}(1)$ is the final coordinate of the particle under consideration after traversing a lens. The similar transformation matrix R can be used for all particles traversing a given element one particle differing from another only by its initial coordinate vector [1]. The ion optical line with interspersing drift spaces can be described using the same basic equation with R being replaced by the product matrix $R(t) = R(n)...R(3)R(2)R(1)$ of the individual matrices of the system elements in conjunction with the drift space between them. The cumulative matrix R can be utilized to compute several trajectories using TRANSPORT code [1] or any other available tool that can perform linear transformation. Fundamentally, Eq. (3.2) can be written in matrix form with cumulative matrix R as follows [34],

$$\begin{bmatrix} x_1 \\ x_1' \\ y_1 \\ y_1' \\ z_1 \\ p_{z_1} \end{bmatrix} = \begin{bmatrix} R_{11} & R_{12} & R_{13} & R_{14} & R_{15} & R_{16} \\ R_{21} & R_{22} & R_{23} & R_{24} & R_{25} & R_{26} \\ R_{31} & R_{32} & R_{33} & R_{34} & R_{35} & R_{36} \\ R_{41} & R_{42} & R_{43} & R_{44} & R_{45} & R_{46} \\ R_{51} & R_{52} & R_{53} & R_{54} & R_{55} & R_{56} \\ R_{61} & R_{62} & R_{63} & R_{64} & R_{65} & R_{66} \end{bmatrix} \begin{bmatrix} x_0 \\ x_0' \\ y_0 \\ y_0' \\ z_0 \\ p_{z_0} \end{bmatrix} . \tag{3.3}$$

3.1.1 Beam Dynamics in Quadrupole

The quadrupole magnets consist of four iron pole pieces laid out such that in the planar multipole expansion of the field, the dipole terms cancel and where the lowest significant terms in the field are quadrupole [21]. The magnetic fields produced by such magnets are hyperbolically shaped. This is due to the fact that the pole pieces of quadrupole magnets are also hyperbolically shaped as shown in figure 3.1. One can consider the equation of motion for a particle in a

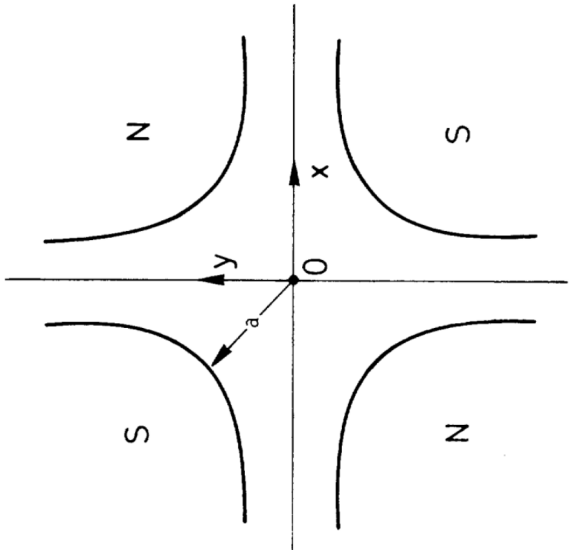

Figure 3.1: Cross-section of a quadrupole magnet.

positive quadrupole field (see [35])

$$\frac{d^2x}{dz^2} + kx = 0 \ , \tag{3.4}$$

$$\frac{d^2y}{dz^2} - ky = 0 \ , \tag{3.5}$$

where the parameter $k^2 = G/B\rho$ is the quadrupole strength

- $G = B_0/a$ is the magnetic-field gradient and B_0 is the magnetic field at radius a.
- a is the radius of the aperture.
- $B\rho$ is the magnetic rigidity of the particle.

The solutions for Eq. (3.4) and (3.5) can be resolved to

$$\begin{aligned} x &= (cos\ kl)\ x_0 + \frac{(sin\ kl)}{k}\ x_0' \\ x' &= (-k\ sin\ kl)\ x_0 + (cos\ kl)\ x_0' \\ y &= (cosh\ kl)\ y_0 + \frac{(sinh\ kl)}{k}\ y_0' \\ y' &= (k\ sinh\ kl)\ y_0 + \ (cosh\ kl)\ y_0' \end{aligned} \tag{3.6}$$

where l is the effective length of the quadrupole and in essence $k = \sqrt{\frac{B_0}{aB\rho}}$. These solutions are for a quadrupole which focuses in the

horizontal (x) plane and defocuses in the vertical (y) plane. From the equations in (3.6) one can write first-order quadrupole magnet transfer matrix as [1, 35]:

$$R_{quad} = \begin{bmatrix} cos\ kl & (1/k)sin\ kl & 0 & 0 & 0 & 0 \\ -k\ sin\ kl & cos\ kl & 0 & 0 & 0 & 0 \\ 0 & 0 & cosh\ kl & (1/k)\ sinh\ kl & 0 & 0 \\ 0 & 0 & k\ sinh\ kl & cosh\ kl & 0 & 0 \\ 0 & 0 & 0 & 0 & 1 & 0 \\ 0 & 0 & 0 & 0 & 0 & 1 \end{bmatrix}. \tag{3.7}$$

From the above matrix, it is clear that a quadrupole magnet can only focus in one transverse direction while defocusing on the other. The quadrupole represented by the 6×6 matrix in Eq. (3.7) focuses in the x direction. Changing the focusing plane would require one to interchange the first two diagonal submatrices. In order to achieve focusing of the beam in both directions using quadrupoles one would need to utilize at least two or more quadrupole magnets placed together. This is the reason why most of the time quadrupoles are arranged in doublets or triplets.

3.1.2 Beam Dynamics in Solenoid

A solenoid is a type of electromagnet whose purpose is to generate a controlled magnetic field through a coil wound into a tightly packed helix as illustrated in figure 3.2. It is one of the electromagnets that are often used to focus charged particle beams in the LEBT. Solenoids

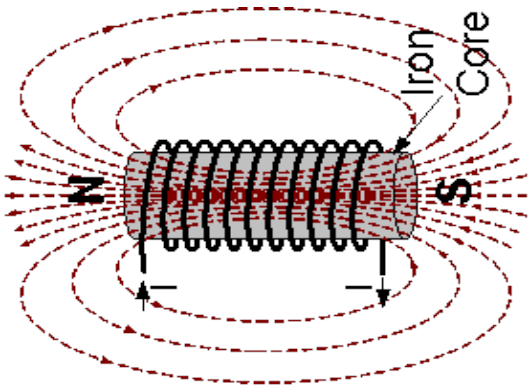

Figure 3.2: Magnetic field lines of a solenoid magnet [36].

couple the x and y directions and they have a slightly complicated

magnetic field configuration in terms of describing it mathematically. In order to simplify the mathematical approach, one can look at it as a three-piece process also known as short lens approximation [37]. The magnetic field is viewed differently from an entry region (R_1), body region (R_2) and exit region (R_3). At the entry and exit regions one can consider the action of the radial field and in the body region one can consider the action of the longitudinal field. The transfer matrix for the entire solenoid is the product of these three different matrices R_1, R_2 & R_3 and they are given as follows:

$$R_1 = \begin{bmatrix} 1 & 0 & 0 & 0 \\ 0 & 1 & k & 0 \\ 0 & 0 & 1 & 0 \\ -k & 0 & 0 & 1 \end{bmatrix}, R_3 = \begin{bmatrix} 1 & 0 & 0 & 0 \\ 0 & 1 & -k & 0 \\ 0 & 0 & 1 & 0 \\ k & 0 & 0 & 1 \end{bmatrix},$$
$$R_2 = \begin{bmatrix} 1 & (1/2k)sin\ 2kl & 0 & (1/2k)(1 - cos\ 2kl) \\ 0 & cos\ 2kl & 0 & sin\ 2kl \\ 0 & -(1/2k)(1 - cos\ 2kl) & 1 & (1/2k)sin\ 2kl \\ 0 & -sin\ 2kl & 0 & cos\ 2kl \end{bmatrix}. \tag{3.8}$$

The first-order solenoid magnet transfer matrix is a product of the three matrices $R_{solenoid} = R_3 \cdot R_2 \cdot R_1$ and can be written as [1, 37]:

$$R_{solenoid} = \begin{bmatrix} C^2 & \frac{1}{k}SC & SC & \frac{1}{k}S^2 \\ -kSC & C^2 & -kS^2 & SC \\ -SC & -\frac{1}{k}S^2 & C^2 & \frac{1}{k}SC \\ kS^2 & -SC & -kSC & C^2 \end{bmatrix}, \tag{3.9}$$

where $C = coskl, S = sinkl$, l is the effective length of the solenoid, $k = B_0/2B\rho$ and B_0 is the magnetic field inside the solenoid. The 6D transfer matrix for the solenoid is given as [1]:

$$R_{solenoid} = \begin{bmatrix} C^2 & \frac{1}{k}SC & SC & \frac{1}{k}S^2 & 0 & 0 \\ -kSC & C^2 & -kS^2 & SC & 0 & 0 \\ -SC & -\frac{1}{k}S^2 & C^2 & \frac{1}{k}SC & 0 & 0 \\ kS^2 & -SC & -kSC & C^2 & 0 & 0 \\ 0 & 0 & 0 & 0 & 1 & 0 \\ 0 & 0 & 0 & 0 & 0 & 1 \end{bmatrix}. \tag{3.10}$$

3.1.3 Drift Space

The drift space is the field free region in the beamline. The particle beams roam freely here, with the displacement and speed perpendicular to the z-direction being assumed to be negligible in collation with the z direction and speed. The first-order transfer matrix for the drift space of length L is given as [1, 33],

$$R_L = \begin{bmatrix} 1 & L & 0 & 0 & 0 & 0 \\ 0 & 1 & 0 & 0 & 0 & 0 \\ 0 & 0 & 1 & L & 0 & 0 \\ 0 & 0 & 0 & 1 & 0 & 0 \\ 0 & 0 & 0 & 0 & 1 & 0 \\ 0 & 0 & 0 & 0 & 0 & 1 \end{bmatrix}. \tag{3.11}$$

3.1.4 Liouville's Theorem

Theoretically one can deal with a problem of how to trace the path of a single particle going through an optical system. However, practically it is different because particles travels as a cloud of particles. One must deal with this cloud of particles by describing their motion in phase space. Sturm Liouville provided a powerful tool for this. If one consider a complex system of N particles with coordinates $(q_1(t), ...q_N, p_1(t), ...p_N(t))$ where q is a position and p is the momentum. Conservative systems can be described by the Hamiltonian $H(q_1, ...q_N, p_1, ...p_N, t)$. The Hamiltonian equation describes the evolution of the system [34, 38]:

$$\dot{q}_i = \frac{\partial H}{\partial p_i}, \quad \dot{p}_i = -\frac{\partial H}{\partial q_i}, \tag{3.12}$$

where $\dot{q}$ is the derivative of q with respect to the time t. Allowing $\Psi(q_1, ...q_N, p_1, ...p_N, t)$ to be the phase space density at a time t. The total derivative of Ψ with respect to time is:

$$\begin{aligned} \frac{d\Psi}{dt} &= \frac{\partial \Psi}{\partial t} + \sum_i \frac{\partial \Psi \partial q_i}{\partial q_i \partial t} + \sum_i \frac{\partial \Psi \partial p_i}{\partial p_i \partial t} \\ &= \frac{\partial \Psi}{\partial t} + \sum_i \dot{q}_i \frac{\partial \Psi}{\partial q_i} + \sum_i \dot{p}_i \frac{\partial \Psi}{\partial p_i}. \end{aligned} \tag{3.13}$$

By making use of the equation of continuity

$$\frac{\partial \Psi}{\partial t} + \nabla(\psi \mathbf{v}) = 0, \tag{3.14}$$

where $\mathbf{v} = (\dot{q_1}, ..., \dot{q_N}, ..., \dot{p_1}, ..., \dot{p_N})$, it can be depicted that the total time derivative of Ψ disappears:

$$\begin{aligned} 0 &= \frac{\partial \Psi}{\partial t} + \nabla(\psi \mathbf{v}) \\ &= \frac{\partial \Psi}{\partial t} + \sum_i \dot{q_i} \frac{\partial \Psi}{\partial q_i} + \sum_i \dot{p_i} \frac{\partial \Psi}{\partial p_i} + \psi \sum_i \left(\frac{\partial \dot{q_i}}{\partial q_i} + \frac{\partial \dot{p_i}}{\partial p_i} \right) \\ &= \frac{\partial \Psi}{\partial t} + \sum_i \dot{q_i} \frac{\partial \Psi}{\partial q_i} + \sum_i \dot{p_i} \frac{\partial \Psi}{\partial p_i} + \psi \sum_i \underbrace{\left(\frac{\partial}{\partial q_i} \frac{\partial H}{\partial p_i} - \frac{\partial}{\partial p_i} \frac{\partial H}{\partial q_i} \right)}_{=0}. \end{aligned} \tag{3.15}$$

This is Liouville's theorem, which states that under the influence of conservative forces the particle density in phase space remain constant [2]. Now, it can be shown that a volume V of a phase space transforms as

$$V_f = \det \mathbf{R} \cdot V_i, \tag{3.16}$$

where V_i and V_f are the initial and final volume, and $\mathbf{R}$ represent the transfer matrix defined in Eq. (3.3) of the beamline. By the use of Liouville theorem, this volume will remain constant for as long as particles are experiencing static magnetic field, therefore

$$\det \mathbf{R} = 1. \tag{3.17}$$

This outcome is only valid when using coordinates defined in Eq. (3.1). The coordinates should be canonically conjugated i.e. the particle momentum is kept constant.

3.1.5 Beam Matrix

It is conventional for one to consider the beam of particles as a cloud of points enclosed by an elliptical contour in (x, x') phase space. This beam of particles, following Liouville's theorem, obeys the conservation law on the phase space [39] described by

$$\gamma x^2 + 2\alpha x x' + \beta x'^2 = \mathcal{E}_x, \tag{3.18}$$

where β, α and γ are the ellipse parameters also known as Twiss parameters and $\mathcal{E}_x$ is the emittance in the horizontal plane. The $\mathcal{E}$ refers to the root mean square emittance ($\mathcal{E}_{rms,x}$) which means 60% of the particles in the beam are considered but for conventional purposes $\mathcal{E}_x$ would be used thoughout this work. The Twiss parameters describe the projections of the beam distribution onto the phase space planes as illustrated in figure 3.3 and β, α and γ are connected by the relation

$$\gamma = \frac{1+\alpha^2}{\beta}. \tag{3.19}$$

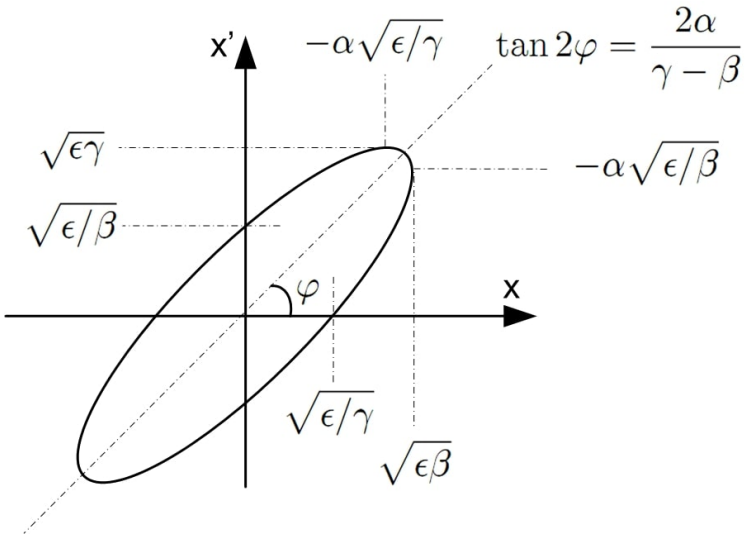

Figure 3.3: Ellipse defining the beam emittance in (x, x') phase space [40]

The same representation applies for (y, y') phase space. The equation of an ellipse in phase space can be represented by introducing symmetric two dimensional beam matrix σ [34]:

$$\begin{bmatrix} x & x' \end{bmatrix} \begin{bmatrix} \sigma_{11} & \sigma_{12} \\ \sigma_{12} & \sigma_{22} \end{bmatrix}^{-1} \begin{bmatrix} x \\ x' \end{bmatrix} = X^T \sigma^{-1} X = 1. \tag{3.20}$$

The horizontal beam width in this case is represented by $\sqrt{\sigma_{11}}$. Because of the symmetrical nature of the beam matrix element σ_{21} is equal to σ_{12}. Then Eq.(3.18) can also be written as

$$\sigma_{22}x^2 - 2\sigma_{12}xx' + \sigma_{11}x'^2 = \det \sigma. \tag{3.21}$$

Comparing Eq. (3.21) with Eq. (3.18) one can deduce the following relations between the Twiss parameters, the emittance and the beam matrix:

$$\sigma = \begin{bmatrix} \sigma_{11} & \sigma_{12} \\ \sigma_{12} & \sigma_{22} \end{bmatrix} = \mathcal{E} \cdot \begin{bmatrix} \beta & -\alpha \\ -\alpha & \gamma \end{bmatrix}, \tag{3.22}$$

$$\mathcal{E} = \sqrt{det\ \sigma} = \sqrt{\sigma_{11}\sigma_{22} - \sigma_{12}^2}. \tag{3.23}$$

One can write beam matrix elements normalized by emittance as follows: $\alpha \equiv -\sigma_{12}/\mathcal{E}$, $\beta \equiv \sigma_{11}/\mathcal{E}$ and $\gamma \equiv \sigma_{22}/\mathcal{E}$. Using this formalism and Eq. (3.17), the equation of the beam ellipse can be written as

$$\sigma_{22}x^2 - 2\sigma_{12}xx^{'} + \sigma_{11}x^{'2} = \mathcal{E}^2. \tag{3.24}$$

From the relation made above between the Twiss parameters and beam matrix elements, one can now represent an ellipse defining the beam emittance by using sigma (σ) notation as illustrated in figure 3.4.

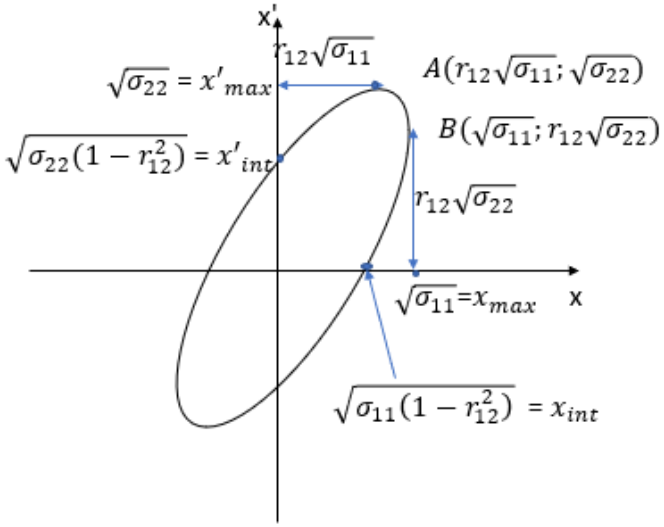

Figure 3.4: A beam ellipse based on the σ matrix in the horizontal phase space [41] with correlation r_{12} which measures the tilt of the ellipse.

The density distribution of a beam can be characterized by using a quadratic function of the phase space variable $\rho(x, x') = \rho(x^T\sigma^{-1}x)$. This density function ρ is a Gaussian [42]:

$$\rho(x, x^{'}) = Nexp\Big[\frac{-(\sigma_{22}x^2 - 2\sigma_{12}xx^{'} + \sigma_{11}x^{'2})}{2\ det\ \sigma}\Big], \tag{3.25}$$

with

$$det\ \sigma = \begin{vmatrix} \sigma_{11} & \sigma_{12} \\ \sigma_{12} & \sigma_{22} \end{vmatrix}.$$

By integrating ρ over x', the matrix elements are taken to be the second moments of the distribution *i.e*, $\sqrt{\sigma_{11}}$ is just the standard deviation of the distribution in x. As mentioned before, when a single particle is transported through the beamline whose components are defined by a transfer matrix, the phase space coordinate in the final position can be described by Eq. (3.1). Now in 2D phase space it can be described as

$$\mathbf{X(1)} = \mathbf{RX(0)} \text{ with R} = \begin{bmatrix} R_{11} & R_{12} \\ R_{21} & R_{22} \end{bmatrix}. \tag{3.26}$$

The concept of finding emittance can be generalized from two dimensional up to n-dimensional phase space. In this case particles are enclosed by an n-dimensional hyper-ellipsoid instead of an ellipse. The generalized equation for this hyper-ellipsoid is given by [42]

$$X_{nD}^{T} \sigma^{nD^{-1}} X_{nD} = 1, \tag{3.27}$$

where σ^{nD} is the symmetric $n \times n$ beam matrix and X_{nD} denotes an n dimensional coordinate vector. Then n-dimensional emittance can be given by,

$$\mathcal{E}^{nD} = \sqrt{det\ \sigma^{nD}} \tag{3.28}$$

Since the beam of the particles is characterized in detail by its density in the six-dimensional phase space. The beam matrix from the initial position to final position can be calculated by inserting identities $I = R^{-1}R = R^{T}(R^{T})^{-1}$ into Eq. (3.27)

$$\begin{aligned} X_0^T R^T (R^T)^{-1} \sigma_0^{-1} R^{-1} R X_0 &= 1 \\ (RX_0)^T (R\sigma_0 R^T)^{-1} RX_0 &= 1 \\ X^T (R\sigma_0 R^T)^{-1} X &= 1. \end{aligned} \tag{3.29}$$

From the above equation it follows that the beam matrix at the particular position can be related to the beam matrix at any other position as follows:

$$\sigma^1 = R\sigma^0 R^T, \tag{3.30}$$

where R^T is the transpose of transfer matrix R. When considering the transverse beam emittance, it is enough to consider beam matrix in

4D. The projection of the volume of the six-dimensional ellipsoid over the transverse planes leads to the 4×4 beam matrix, which describes the dimensions of the projected beam in the transverse phase space [43];

$$\sigma^{4D} = \begin{bmatrix} \langle x^2 \rangle & \langle xx' \rangle & \langle xy \rangle & \langle xy' \rangle \\ \langle xx' \rangle & \langle x'^2 \rangle & \langle x'y \rangle & \langle x'y' \rangle \\ \langle xy \rangle & \langle x'y \rangle & \langle y^2 \rangle & \langle yy' \rangle \\ \langle xy' \rangle & \langle x'y' \rangle & \langle yy' \rangle & \langle y'^2 \rangle \end{bmatrix} = \begin{bmatrix} \sigma_{11} & \sigma_{12} & \sigma_{13} & \sigma_{14} \\ \sigma_{21} & \sigma_{22} & \sigma_{23} & \sigma_{24} \\ \sigma_{31} & \sigma_{32} & \sigma_{33} & \sigma_{34} \\ \sigma_{41} & \sigma_{42} & \sigma_{43} & \sigma_{44} \end{bmatrix} = \begin{bmatrix} \sigma_{xx} & \sigma_{xy} \\ \sigma_{xy}^T & \sigma_{yy} \end{bmatrix}, \tag{3.31}$$

where σ_{xx}, σ_{xy},σ_{yy} are 2x2 matrices, e.g.

$$\sigma_{xx} = \begin{bmatrix} \sigma_{11} & \sigma_{12} \\ \sigma_{21} & \sigma_{22} \end{bmatrix}. \tag{3.32}$$

The 2D horizontal and vertical motions are characterized by matrices σ_{xx} and σ_{yy} whereas σ_{xy} describes the coupling of x and y. In an event that the beam is transversely uncoupled $\sigma_{xy} = 0$, the 2D beam matrices are adequate to describe the beam. From the 2D matrices, the emittances and Twiss parameters can be acquired using the following [44, 45],

$$\mathcal{E}_\eta = \sqrt{det\ \sigma_{\eta\eta}}, \tag{3.33}$$

$$\begin{aligned} \beta_\eta &= \langle \eta^2 \rangle / \mathcal{E}_\eta \\ \gamma_\eta &= \langle \eta'^2 \rangle / \mathcal{E}_\eta \\ \alpha_\eta &= -\langle \eta\eta' \rangle / \mathcal{E}_\eta \end{aligned} \tag{3.34}$$

where η refers to either x or y.

3.2 4D Transverse Beam Characterization

The transverse emittance is defined in terms of the area occupied by the beam in two-dimensional phase spaces (x, x') and (y, y'). When a profile monitor intercepts the whole beam, only the space width is determined at that point. One can use these beam widths to infer beam emittances. If a beam has matrix σ^0 at some point, z_0 and matrix σ^1 at some other point, z_1, downstream, the transformation of

the beam between z_0 and z_1 can be characterized by a transfer matrix R [46].

One can consider the transverse space only, by dropping longitudinal space elements in Eq. (3.3), so the 6×6 transfer matrix will reduce to a 4×4 transfer matrix. The resulting matrix is,

$$R = \begin{bmatrix} R_{11} & R_{12} & R_{13} & R_{14} \\ R_{21} & R_{22} & R_{23} & R_{24} \\ R_{31} & R_{32} & R_{33} & R_{34} \\ R_{41} & R_{42} & R_{43} & R_{44} \end{bmatrix}. \tag{3.35}$$

Since the beam property that one can measure at a given point is the beam width, x and y, which are respectively related to elements σ^1_{11} and σ^1_{33} of the sigma matrix σ^1, using Eq. (3.30) and Eq. (3.31) by matrix linear transformation, we can express these elements as a function of σ^0:

$$\begin{aligned}\sigma^1_{11} =& R^2_{11}\sigma^0_{11} + 2R_{11}R_{12}\sigma^0_{21} + 2R_{11}R_{13}\sigma^0_{31} + 2R_{11}R_{14}\sigma^0_{41} + R^2_{12}\sigma^0_{22} + \\ & 2R_{12}R_{14}\sigma^0_{42} + 2R_{12}R_{13}\sigma^0_{32} + 2R_{13}R_{14}\sigma^0_{43} + R^2_{13}\sigma^0_{33} + R^2_{14}\sigma^0_{44}\end{aligned} \tag{3.36}$$

and

$$\begin{aligned}\sigma^1_{33} =& R^2_{31}\sigma^0_{11} + 2R_{31}R_{32}\sigma^0_{21} + 2R_{31}R_{33}\sigma^0_{31} + 2R_{31}R_{34}\sigma^0_{41} + R^2_{32}\sigma^0_{22} + \\ & 2R_{32}R_{34}\sigma^0_{42} + 2R_{32}R_{33}\sigma^0_{32} + 2R_{33}R_{34}\sigma^0_{43} + R^2_{33}\sigma^0_{33} + R^2_{34}\sigma^0_{44}.\end{aligned} \tag{3.37}$$

The square root of these two elements of beam matrix σ^1_{11} and σ^1_{33} respectively gives the horizontal and vertical beam widths. The elements of σ^0 can be deduced from a set of several measurements of σ^1_{11} and σ^1_{33} obtained from the beam conditions affected by those different transfer matrices. From the acquired beam matrix elements the transverse beam emittance at z_0 can be deduced. This is the method that is employed in this study to calculate beam emittances.

3.3 Methods for Measuring Beam Emittance

There are several methods that can be applied to measure beam emittance. One can use slit-grid method, pepperpot method, three gradient method, multiple monitors method, etc. In this subsection only three methods are discussed namely; the multiple monitors method, three gradient method and ten gradient method.

3.3.1 Multiple Profile Monitors

One can use multiple profile monitors whereby beam width is measured at several locations along the beamline, z_i, separated by drift spaces [47]. Ordinarily, one can have a profile monitor on position z_0 and on this given position, the beam matrix can be defined as σ^0. The width of the beam in x gives us σ^o_{11}. The following monitor downstream at point z_1 where the beam matrix is σ^1. The transfer matrix for a drift of length $L_1 = z_1 - z_o$ is

$$R_L = \begin{bmatrix} 1 & L_1 & 0 & 0 \\ 0 & 1 & 0 & 0 \\ 0 & 0 & 1 & L_1 \\ 0 & 0 & 0 & 1 \end{bmatrix}. \tag{3.38}$$

Then by using this transfer matrix in Eq. (3.30) reduces to:

$$\sigma^1_{11} = \sigma^0_{11} + 2L_1\sigma^0_{12} + L_1^2\sigma^0_{22}. \tag{3.39}$$

A set of σ^i_{11} corresponding to several different L_i as shown in figure 3.5 forms the system of equations from which the elements of σ^0 are extracted. Then emittance $\mathcal{E}_x$ at z_0 can be calculated using Eq. (3.23). The same procedure can be followed to determine emittance in the y direction.

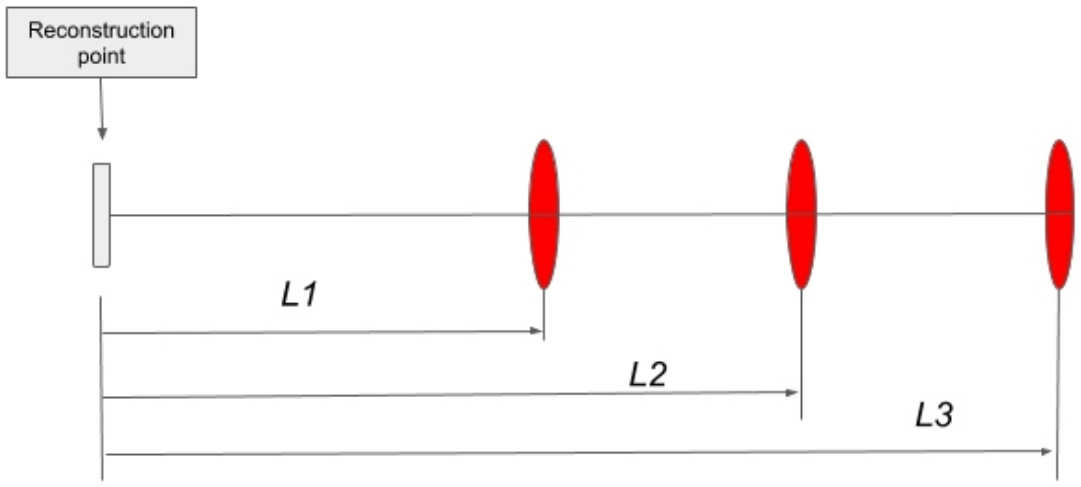

Figure 3.5: The schematic diagram showing the multiple profile monitors placed at different positions with different lengths from a measuring point.

3.3.2 Varying Quadrupole Strengths

Another method involves varying the quadrupole strength in order to change the transfer matrix elements. This change causes the effect of transfer matrix on the particles to change, resulting in different beam profile being measured. A quadrupole 6×6 transfer matrix shown in Eq. (3.7) can be reduced to 4×4 a transfer matrix as given below,

$$R_{quad} = \begin{bmatrix} cos\ kl & \frac{1}{k}\ sin\ kl & 0 & 0 \\ -k\ sin\ kl & cos\ kl & 0 & 0 \\ 0 & 0 & cosh\ kl & \frac{1}{k}\ sinh\ kl \\ 0 & 0 & k\ sinh\ kl & cosh\ kl \end{bmatrix}. \tag{3.40}$$

Then, if the beam profile monitor is placed a distance L downstream from the quadrupole lens. The matrix expressing the beam transformation from the entrance of the quadrupole to the monitor will be given by the matrix product, $Q = R_L R_{quad}$. By making use of Eqs. (3.36) and (3.37) the following equations are yielded.

$$\sigma_{11}^1 = Q_{11}^2\sigma_{11}^0 + 2Q_{11}R_{12}\sigma_{12}^0 + Q_{12}^2\sigma_{22}^0 \tag{3.41}$$

and

$$\sigma_{33}^1 = Q_{33}^2\sigma_{33}^0 + 2Q_{33}R_{34}\sigma_{34}^0 + Q_{34}^2\sigma_{44}^0 \tag{3.42}$$

where Q's explicitly denotes the product of quadrupole matrix multiplied by drift space matrix. Above equations have three unknowns that need to be deduce which means that in order to solve the equations a minimum of **three measurements** of σ_{11}^1 and σ_{33}^1 are required to solve σ^0 obtained from the beam exposed to different transfer matrices. Then the 4×4 σ obtained can be used to calculate transverse emittances $\mathcal{E}_x$ and $\mathcal{E}_y$ using Eq. (3.23).

3.3.3 Varying Solenoid Strengths

Moreover, one can also alter solenoid strength to cause the transfer matrix to change. From Eq.(3.10) the 6×6 solenoid transfer matrix can be also be reduced to a 4×4 transfer matrix given as

$$R_{solenoid} = \begin{bmatrix} C^2 & \frac{1}{k}SC & SC & \frac{1}{k}S^2 \\ -kSC & C^2 & -kS^2 & SC \\ -SC & -\frac{1}{k}S^2 & C^2 & \frac{1}{k}SC \\ kS^2 & -SC & -kSC & C^2 \end{bmatrix}. \tag{3.43}$$

With solenoids the particle beam is rotated as it traverses through it. The matrix expressing the beam transformation from two solenoids separated by distance L_1 between them, with beam profile monitor placed a distance L_2 downstream of the second solenoid is given by $S = R_{L_2} R_{solenoid_2} R_{L_1} R_{solenoid_1}$. A similar approach used in acquiring the σ_{11} and σ_{33} equations on varying quadrupole was adopted. By making use of Eqs. (3.36) and (3.37) the following equations are yielded.

$$\begin{aligned}\sigma_{11}^1 =& S_{11}^2\sigma_{11}^0 + 2S_{11}S_{12}\sigma_{21}^0 + 2S_{11}S_{13}\sigma_{31}^0 + 2S_{11}S_{14}\sigma_{41}^0 + S_{12}^2\sigma_{22}^0 + \\ & 2S_{12}S_{14}\sigma_{42}^0 + 2S_{12}S_{13}\sigma_{32}^0 + 2S_{13}S_{14}\sigma_{43}^0 + S_{13}^2\sigma_{33}^0 + S_{14}^2\sigma_{44}^0\end{aligned} \tag{3.44}$$

and

$$\begin{aligned}\sigma_{33}^1 =& S_{31}^2\sigma_{11}^0 + 2S_{31}S_{32}\sigma_{21}^0 + 2S_{31}S_{33}\sigma_{31}^0 + 2S_{31}S_{34}\sigma_{41}^0 + S_{32}^2\sigma_{22}^0 + \\ & 2S_{32}S_{34}\sigma_{42}^0 + 2S_{32}S_{33}\sigma_{32}^0 + 2S_{33}S_{34}\sigma_{43}^0 + S_{33}^2\sigma_{33}^0 + S_{34}^2\sigma_{44}^0.\end{aligned} \tag{3.45}$$

where $S's$ characterizes the product of solenoids multiplied by drift spaces accordingly. Now, the above equations have ten unknowns that need to be deduced which means that in order to solve the equations a minimum of **ten measurements** of σ_{11}^1 and σ_{33}^1 are required to solve σ^0 obtained from the beam exposed to different transfer matrices. Then the 4x4 matrix σ obtained can be used to calculate transverse beam emittances $\mathcal{E}_x$ and $\mathcal{E}_y$ using Eq. (3.23).

Chapter 4

Experimental and Computational Methods

The fundamental tools for beam emittance measurements are discussed in this chapter. Beam diagnostics equipment to be used for beam profiling and beam intensity measurements are introduced. The basic attributes of the developed emittance calculator are also discussed. The practical procedures for performing both quadrupole and solenoid techniques are explained.

4.1 Beam Diagnostics

Beam diagnostics is an essential constituent of any accelerator. These systems are our organs of sense that let us perceive what properties a beam has and how it is behaving in an accelerator. During routine operation of a particle accelerator and its associated beamlines, it is important for an operator to continuously monitor several beam parameters in order to keep the beam in accepted conditions. Such beam parameters include beam intensity/current, beam profile as well as transverse emittance. For a full list of parameters that require monitoring during operation (see [48]). Several tools are used to measure or monitor those parameters. A Faraday cup is one of the devices that can be used to measure beam current. For the beam profile monitoring a multiwire profile scanner can be utilised. One other important beam parameter is the transverse emittance. Its importance lies in the fact that it can be used to inform the operator if the beam extracted from the ion source can be delivered to a target station. Beam

emittance cannot be measured directly, however it must be inferred by using other measurable beam parameters. In the current work, beam profiles from a multiwire profile scanner are used to deduce transverse emittances using the newly developed system. The system is comprised of two techniques, namely, solenoid scan and quadrupole scan. The reason to choose the two approaches was based on the LEBT at iThemba LABS.

4.1.1 Faraday Cup

As mentioned above, a Faraday cup shown in figure 4.1 is a device used to measure beam intensity in the beamline of a particle accelerator. It was named after Michael Faraday who first theorized ions in 1830 [49]. It is a metal cup which is electrically insulated from its surroundings designed to collect all charged particles in vacuum in the beamline. The resulting current can be used to calculate and determine the amount of ions or electrons that enter the cup.

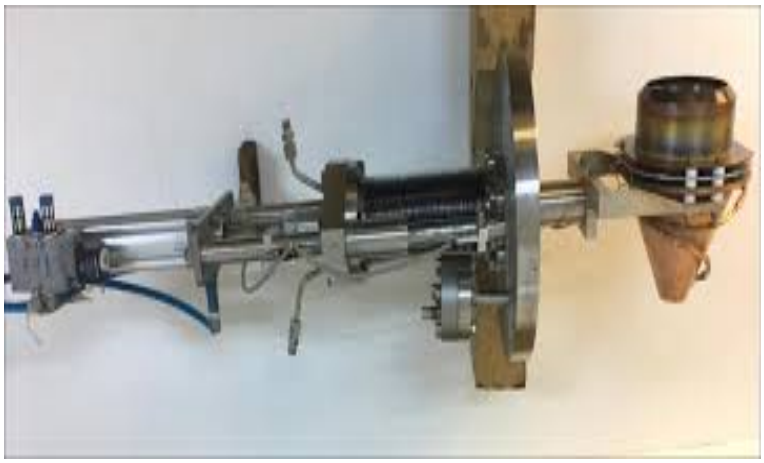

Figure 4.1: A picture of a Faraday cup used to measure beam intensity in the beam pipe [50].

When the beam of charged particles hits the Faraday cup, it gains a small net charge while the ions are neutralized. The current which is equivalent to the number of impinging ions is then measured as the metal cup gets discharged. Fundamentally, the Faraday cup is the part of a circuit where ions in the beamline are the vacuum charge carriers and it acts as an interface to the solid metal where electrons serve as the charge carriers. The number of charges borne by the ions

in the vacuum part of the circuit can be determined by measuring the electric current in the metal part of the circuit [51]. The measured current is directly proportional to the number of ions hitting the metal cup.

4.1.2 Multiwire Profile Scanner (Harp)

A multiwire profile scanner also known as a harp (shown in figure 4.2) is a piece of equipment that is composed of a number of metal wires placed parallel to one another and is used to measure beam profile. One plane of the wires is aligned vertically to measure horizontal profile while the other set of wires are horizontally aligned for measuring vertical profile. Each individual wire is connected to an electrical vacuum feed-through and an amplifier. Usually these wires are made up of copper or tungsten because of their high melting and sublimation temperatures.

The harp is a type of monitor that is capable of measuring the intensity distribution of the beam and its transverse positions. When a beam of charged particles hit the wires, electrons are kicked out from the atoms. This is called secondary electron emission. The more the particles hit the wire, the more secondary electrons are liberated. An electric field is applied orderly to clear the electrons in the vicinity of the wire. This is done so that electron cloud would not form over the surface of wires and impede further emission. Naturally, electric current is generated when free electrons flow in the conductor, and in this case the wire is the conductor. Therefore the electric current flowing in the wire is measured by connecting both ends to a measuring circuit. Consequently by measuring the current arising due to secondary electron emission from the wire, one gets a handle on the particle density at the position of the wire. The process is performed for each wire and the associated current is measured.

Shown in figure 4.2 is the picture of a harp used for beam profile monitoring at iThemba LABS. It has 48 wires in both x and y directions. The wire spacing is in order of 3 mm, 2 mm and 1 mm towards the centre position. There are 12 wires with 3 mm spacing, 14 wires with 2 mm spacing and 20 wires with 1 mm spacing. The interval in the middle of the two end wires is 5 mm and the wires have a length of 87

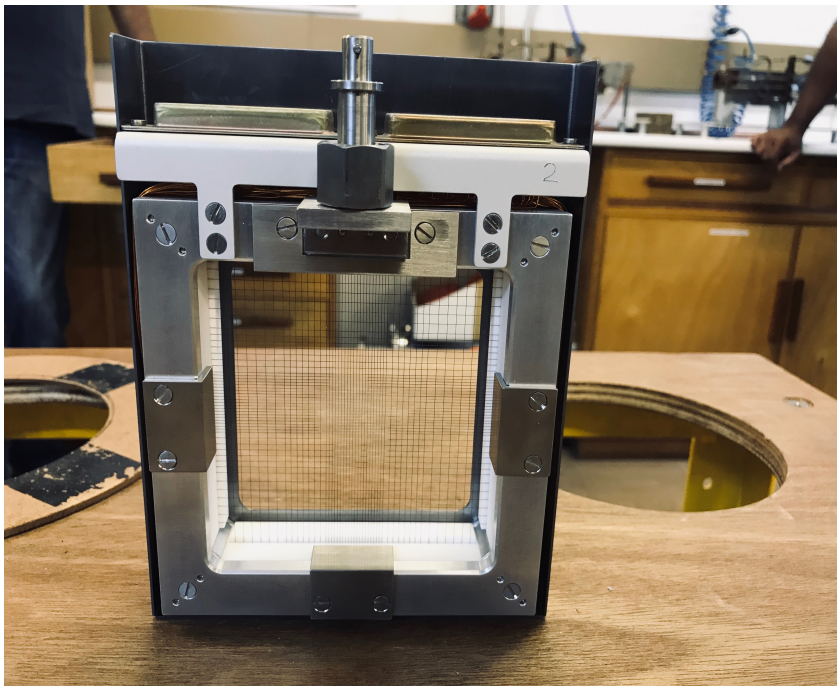

Figure 4.2: The harp with 48 copper wires with a thickness of 20 μm, in both x and y directions used for beam profiling.

mm. Figure 4.3 shows an example of the beam profile when the beam is intercepted by the harp. Left hand side is the horizontal plane (x) while on the right hand side is the vertical plane (y).

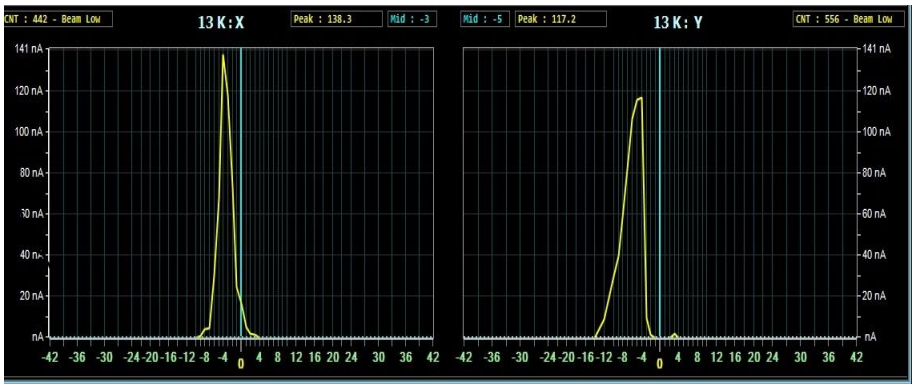

Figure 4.3: This picture shows the beam profiles when the beam is intercepted by the harp.

4.1.3 Development and Testing of the "Emittance Calculator"

The ion source division at iThemba LABS is the one responsible for developing and making of heavy ions beams. In the development pro-

cess, the knowledge of transverse beam emittances and monitoring thereof is important. This is due to the fact that emittance can be used as a tool to inform operator if the beam being extracted from the source is of good quality. At the beginning of this project there was no system that makes it possible to infer beam emittances of the beams from the ECRIS. It was decided that the system which is capable of deducing emittances in LEBT must be developed. During the design stage of the system several stakeholders were involved and it was decided that the system must meet certain requirements. These requirements include:

- The system must be user-friendly.
- It must be compatible with both Windows and Unix based systems.
- The system must be incorporated with the Experimental Physics and Industrial Control System (EPICS).
- Most of the steps required to complete the measurements must be automated.
- The system should display beam ellipses in order for one to check against acceptance of SPC2.

In order to meet the above requirements, several ideas on how to build this robust system were put together. Aspects like which programming language(s) should be used and why were considered. By looking at different packages and libraries that each programming language has, Python and Java were two languages that could be used in developing the envisaged emittance calculator. And for data collection C^{++}, Bash script, EPICS and Python were used and the ROOT package was used for data analysis.

The emittance calculator application was firstly developed using Java programming language. This was achieved by solving Eqs. (3.41, 3.42, 3.44 and 3.45) using Java libraries. At this point of the development, the Q-line emittance inference was being accomplished by using Eqs (3.44 and 3.45). These equations were being solved with utilization of only the transfer matrix of solenoid L5Q matrix and the drift space matrix before and after the magnet with solenoid L4Q excluded. This

was done that way because it was assumed that the emittance from the ECRIS is the same as the one that can be measured at any position between solenoid L4Q and solenoid L5Q. However, the beamline design performed in [28] reported that the LEBT setup was designed such that the emittance from the ECRIS is the same as the one just before solenoid L4Q and $\mathcal{E}_x$ & $\mathcal{E}_y$ must be swapped before the beam is injected into the AX-line. The input parameters that are required by the application were particle's atomic mass, charge state, kinetic energy (E_k), beam widths and magnetic field strengths. Using TRANSPORT simulations the Java application could be tested. Data was uploaded into TRANSPORT and the beam widths were gathered using both solenoid and quadrupole scan methods. The acquired beam widths with associated magnetic field strengths and beam parameters were used on the emittance calculator to compute transverse beam emittance. The calculated emittances were in agreement with the injected ones.

Even though the developed application could reproduce the injected emittances, it was still not calculating emittances extracted from the ion sources. This was due to the exclusion of solenoid L4Q in solving of the transfer matrix. So at this point of the development it was decided that some changes needed to be implemented on the emittance calculator. Firstly, it became necessary to include solenoid L4Q matrix, solenoid L5Q matrix together with the drift spaces on the transfer matrix. Secondly, one of the requirements was to make the system user friendly and at this point it was deemed not completely user friendly. This was due to the fact that for one to fill in the required parameter values on the calculator they have to do it directly within the code which is a time consuming exercise. Therefore the changes were implemented on the application and it was also upgraded to become more dynamic by using a graphical user interface (GUI). The plots showing the beam ellipses on each phase space were also shown on a separate GUI.

The time it took for a user to populate all the required fields to calculate beam emittance was a bit long because it was done manually, then it had to be reduced. To achieve this, the input values required were organized and stored in a text file such that it would be easy to upload data on the emittance calculator. Also, the files needed to

be generated during measurements hence it was crucial to add this functionality. The beam widths along with the magnet's currents are arranged in columns inside the text file. This functionality makes it easy to populate the required fields by simply choosing a text file with the relevant data. At this point of the development making this feature possible using , proved to be a challenging task and the transverse beam ellipses plots were impossible to embed on the emittance calculator without using a different GUI. The decision was then made to change from Java to Python programming language. This choice was motivated by the packages that Python offers which would make it possible to meet all these specifications.

The same logic explained above was followed when using Python to develop the emittance calculator and the end result for this application is as shown in figure 4.4. In this improved version the user has an option of populating all the required fields manually or to use the select button in order to fill in the beam widths and magnet's currents and manually fill in the beam parameters. The user can then click the calculate button to calculate transverse beam emittance, and a plot button to show the beam ellipses on each transverse space.

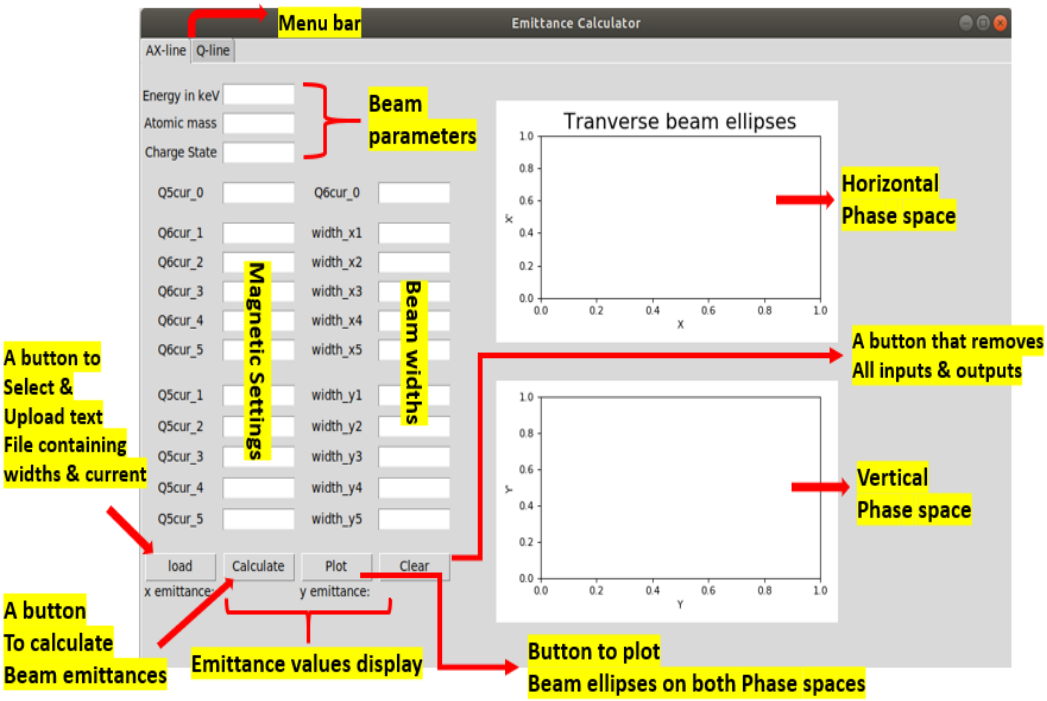

Figure 4.4: The sample of the graphical user interface of the newly developed "Emittance Calculator" system. The text input fields in the GUI are all the required information that the user is expected to insert in order to perform the calculations.

To validate the transverse beam emittance calculated using the developed emittance calculator, TRANSPORT code was used. The Q-line and the AX-line were simulated in TRANSPORT. Different types of beams with known beam emittances were injected. The solenoid and quadrupole scan methods were accordingly employed to gather beam widths. Subsequently, the magnetic field strengths, beam widths, along with beam parameters were accordingly used to calculate beam emittance. The calculated emittances were then compared with the ones injected into TRANSPORT in order to verify if the emittance calculator is working appropriately. During this process some discoveries were made and are as follows:

- The minimum solenoid current step size was discovered to be 1.6 A.
- Solenoid L4Q current has to be changed after the 5^{th} alteration of solenoid L5Q current when acquiring the ten beam widths.
- The relationship between focusing magnetic field and beam widths must be parabolic.

Firstly, when solenoid L5Q is varied in order to get beam widths. The step size should not be less than 1.6 A, because if that is the case, it means that the change in strength is small such that there won't be a difference between the transfer matrices between the two measurements. As a result the beam widths acquired won't be effective in constructing the injected emittance. Secondly, when solenoid L5Q current is varied ten times straight up using 1.6 A step size or greater, the gathered beam widths grow out of proportion. Therefore the ten measurements had to be split into two parts. Which means that solenoid L4Q current has to be fixed at a certain value for the first five measurements and be changed for the remaining five measurements. Thirdly, the importance of the parabolic relationship between the magnet's currents and beam widths. So, the beam widths gathered after performing a quadrupole scan or solenoid scan must be centered around the beam waist such that the magnet's currents vs beam widths relationship is parabolic. This means that as you alter the magnet's currents towards the focal point the beam converges, which means the beam width decreases until it reaches a minimum point

(focused beam). Then it start to diverge whereby the beam widths increases. Therefore, such behaviour must be achieved when performing measurements. If this is not the case the measured beam widths would most likely not be possible to deduce the correct emittances. Then after several interactive processes of improving the system, the transverse beam emittance measurements were then performed on real beams. The results are discussed in chapter 5.

4.2 Emittance measurements procedure

As already discussed, the beam emittance measurements in this work are performed using two of the three techniques discussed in Chapter 3 (i.e **the quadrupole scan and solenoid scan**). For both methods a Gaussian approximation program was developed and used to determine beam widths of the beam profile obtained from the harps. The program was written using C++ programming language and data accumulated was analyzed using the ROOT toolkit. This program gets the current measured against wire identification number. Then it is required to convert wire number to wire position in order to get the actual widths. The Gaussian fit is performed on the plot of beam current measured by each wire against wire positions as shown in figure 4.5 and the beam widths are acquired and saved on a file.

In greater detail the system is designed such that every piece of code needed for the beam width measurements for each methodology is put together in the batch file using a bash scripting language. There are two Batch files compiled; one file is for the quadrupole scan and the other one is for the solenoid scan. When the Batch file for the quadrupole scan is executed the user is prompted to give the following; the file directory where measurements will be saved, direction of beam widths, initial current of the quadrupole and the magnet current step size. The quadrupole currents are then converted to the magnetic field strengths using the calibration curve shown in figure 4.6. This conversion is done so that the quadrupole current in amperes is converted to magnetic field in tesla.

The Gaussian fitting program is used to collect and analyze data and this process is automated. After data collection, the Gaussian fitting is performed and the magnet's currents vs beam widths plot is presented

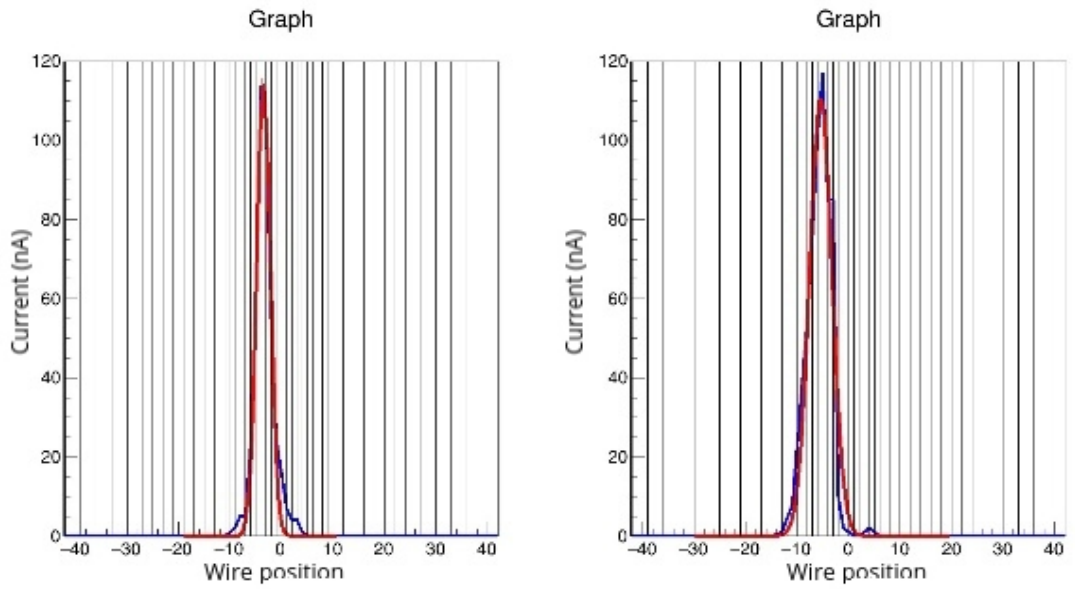

Figure 4.5: Example of beam profiles fitted with Gaussian distribution in order to obtain beam widths in both x (left) and y (right) directions.

to the user. It is expected that the plot must show the parabolic relationship. A user then decides if they approve the results or they want to start over. If they approve, the data is saved in the text file and if they don't, the data can be discarded and the process can be restarted. The saved data files can be easily uploaded in the emittance calculator.

The above procedure is similar to the solenoid scan batch file but in this case the user is not asked for focusing direction due to the fact that the beam width measurements for both directions are performed concurrently. The solenoid currents are also converted to magnetic field using the calibration curve shown in figure 4.7. The results are then further analyzed by the Gaussian fitting program and then they are stored in the text file. Then the obtained results are used to calculate transverse beam emittance using the emittance calculator. The whole processes (quadrupole and solenoid scans) are summed up by two flow charts shown in figures 4.8 and 4.9.

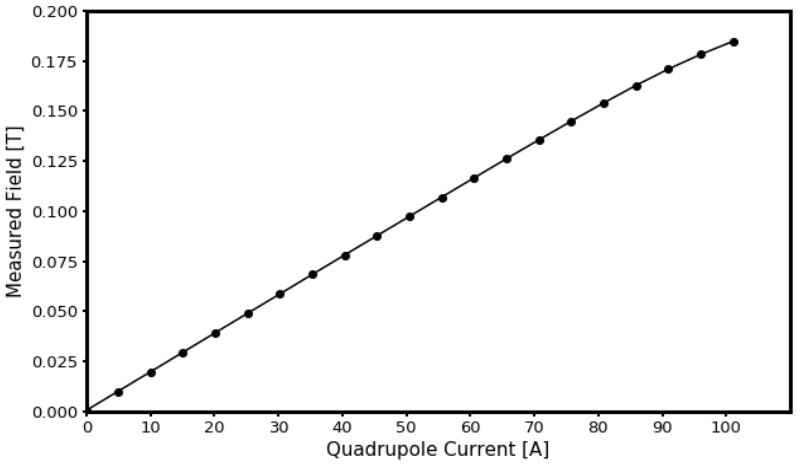

Figure 4.6: The plot showing the calibration curve of the correlation between quadrupole current and the measured magnetic field in tesla.

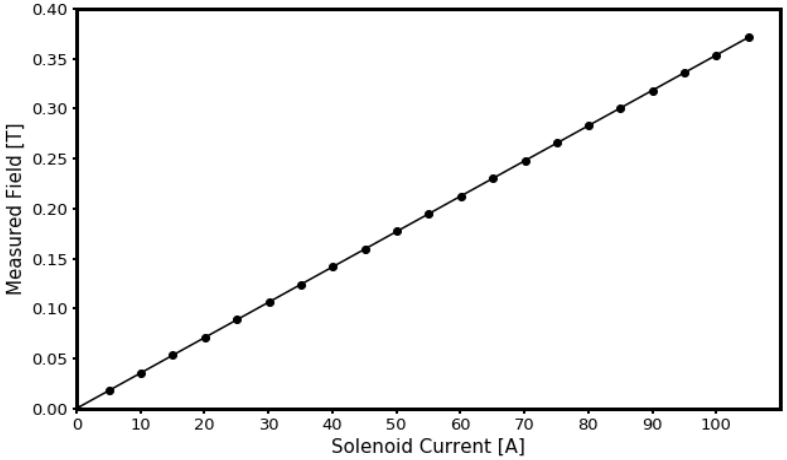

Figure 4.7: The plot showing the calibration curve between current applied to the solenoid and the measured magnetic field in tesla.

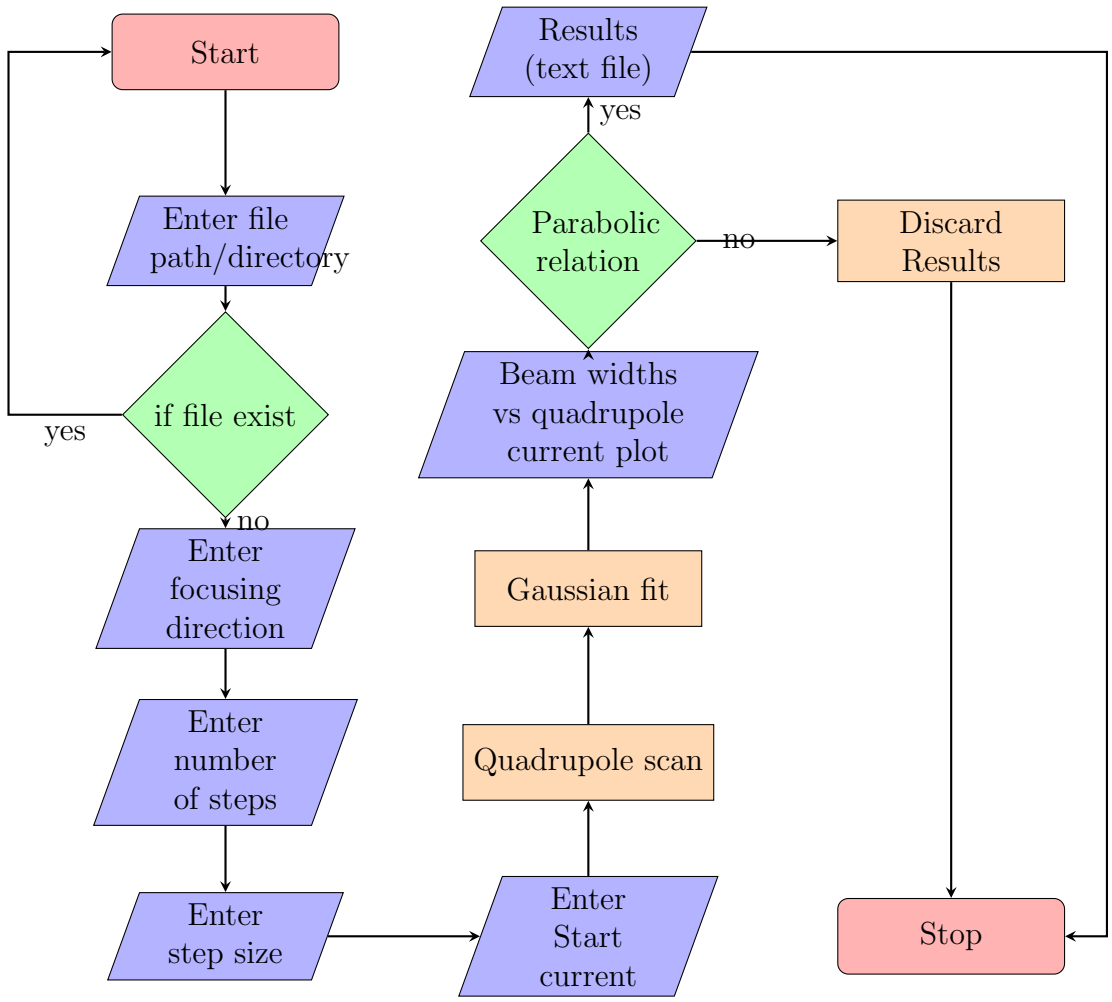

Figure 4.8: Flow chart showing the data collection flow for the quadrupole scan procedure.

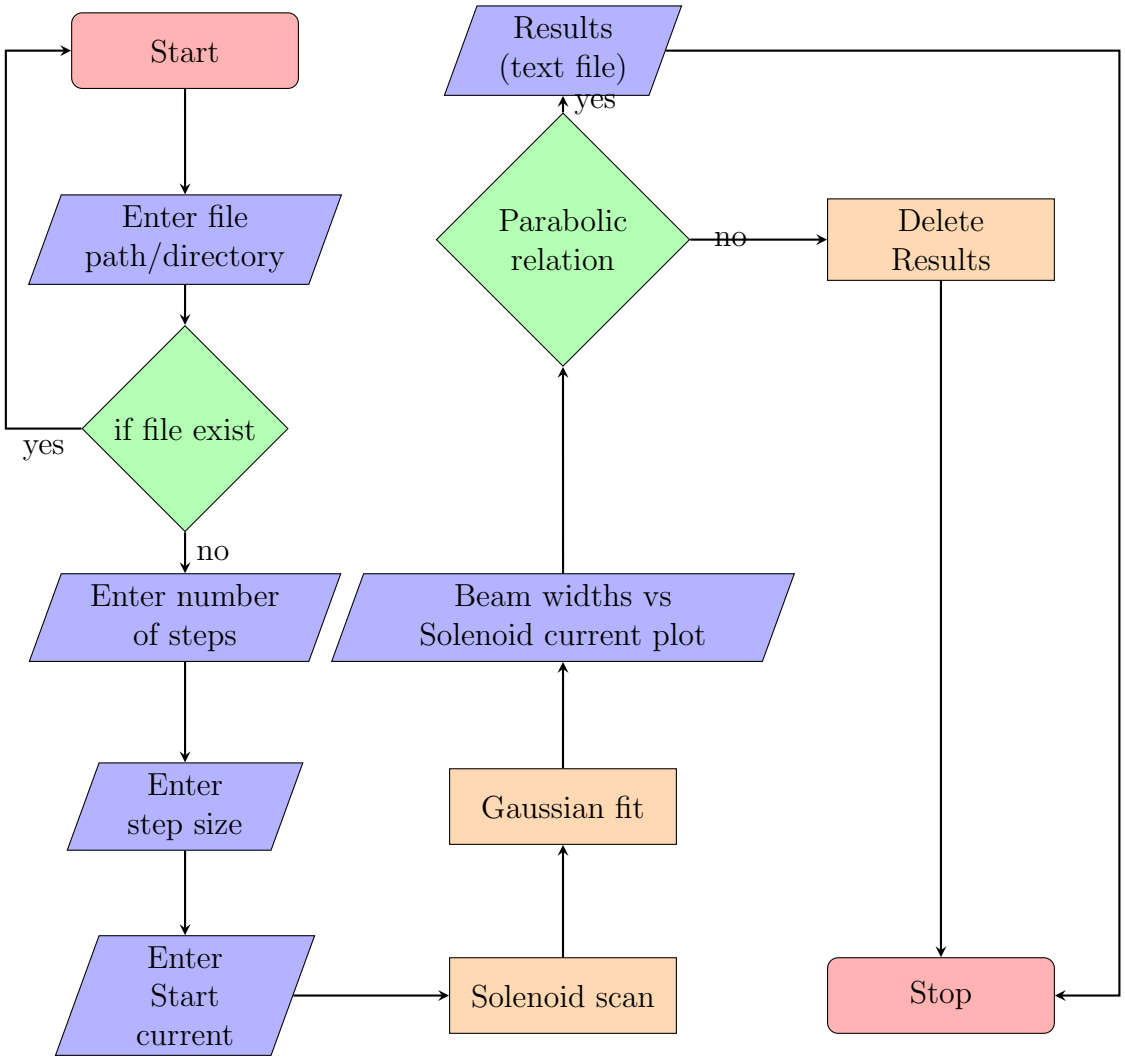

Figure 4.9: Flow chart showing the data collection flow for the solenoid scan procedure.

4.2.1 The Quadrupole and Solenoid Scans

Quadrupole Scan

The emittance measurements in the vertical beamline (AX-line) was accomplished by utilizing the "quadrupole scan". This process involves the use of quadrupoles Q5 and Q6 in conjunction with harp 2AX in the AX beamline section (see figure 2.9). Using harp 2AX as a profile monitor, the beam is tuned such that it is focused to the relative minimum beam size. Then, the current of quadrupole Q5 was varied five times (two steps down from the optimal set point and two steps up from the optimal set point) in order to obtain beams widths for vertical phase space emittance $\mathcal{E}_y$. The current of quadrupole Q6 and other beamline elements are kept constant during this procedure. For horizontal emittance ($\mathcal{E}_x$) measurements quadrupole Q6 was varied five times while keeping quadrupole Q5 and other elements are kept constant. Figure 4.10 is an illustration of how a quadrupole scan affects the beam ellipse at position z where a profile monitor is situated. Also shown in the figure is an example of how the profile will look like if the beam is intercepted with the harp. For both measurements, the beam widths were obtained from a Gaussian fitting program and the emittance $\mathcal{E}_x$ and $\mathcal{E}_y$ were calculated with the emittance calculator.

Solenoid Scan

The similar approach was adopted for Q-line measurements. The "solenoid scan" is achieved by using solenoid L4Q and L5Q in conjunction with harp 5Q (see figure 2.9). Firstly the beam was tuned such that the minimum beam waist is found using harp 5Q as a profile monitor. Then, the solenoid L4Q was fixed at a certain value while solenoid L5Q is varied to get the first five beam widths. For the second five set of beam widths measurements, solenoid L4Q was changed and fixed on another current value and solenoid L5Q was again varied five times. The beam widths were also obtained from a Gaussian fitting program and the emittance $\mathcal{E}_x$ and $\mathcal{E}_y$ were calculated with the emittance calculator.

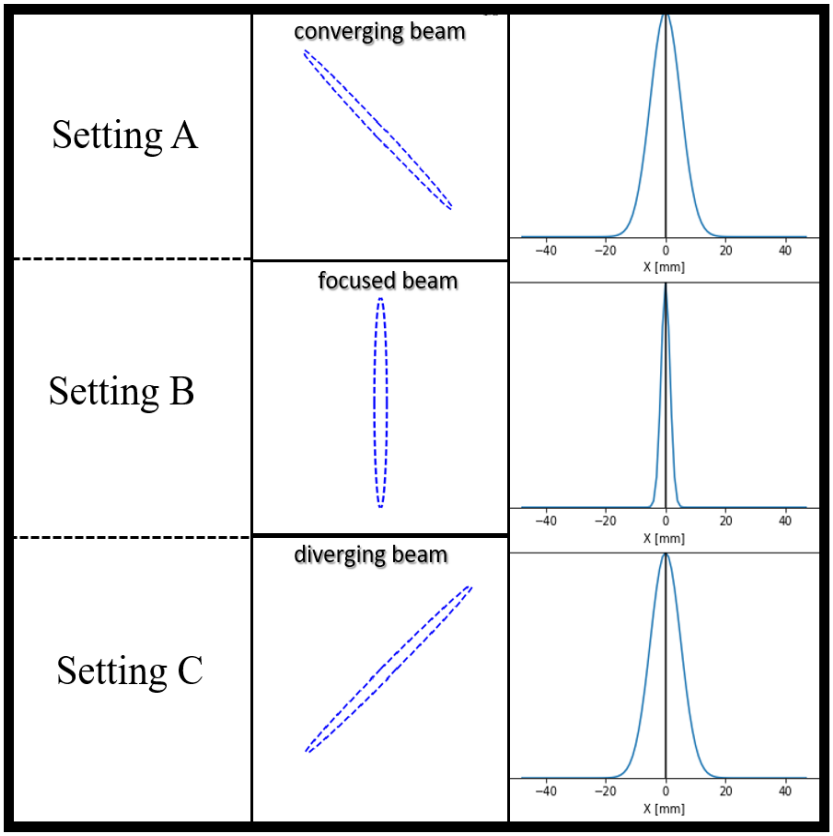

Figure 4.10: Figure showing how a quadrupole scan affect the beam ellipse at position z. Also shown is the related beam profile that can be seen if the beam is intercepted by a harp.

Chapter 5

Results and Discussions

The beam widths obtained from utilizing quadrupole and solenoid scans, on TRANSPORT and by using Gaussian approximation program on measured beam profiles are presented in this chapter. Emittance calculations results acquired using the developed emittance calculator are shown and the beam ellipses on each phase space are also presented. The measurements results are also discussed in detail.

5.1 Emittance Calculator Validation

TRANSPORT code is one of the fundamental tools used for designing non-dynamic magnetic beam transport systems. It is a first and second order matrix multiplication computer program which can be used to investigate various beam properties during the design of beam transport systems. In the current work TRANSPORT was used for benchmarking the newly developed emittance calculator. To do this TRANSPORT was used to obtain beam widths at certain points in the beamline and these widths were inserted into emittance calculator in order to deduce transverse emittances. It must be noted that the beam widths obtained from TRANSPORT are $2.5^{*}\sigma$ which is assumed to be 100% of the particles enclosed in the beam in the specific direction, whereas in rms emittances (which are used in the current study's measurements) widths are $1^{*}\sigma$ which is 68% of particles enclosed in the beam[††].

To benchmark the functionality of the emittance calculator, different

[††]The parameter σ characterizes width of the beam at certain position in the beamline.

types of beams with user defined transverse beam emittance values were injected into the TRANSPORT code. Both the solenoid and quadrupole scans methods were applied in order to calculate beam widths. The obtained beam widths together with the associated beam parameters were used on the emittance calculator to verify if the injected transverse beam emittances could be reproduced.

One of the beams investigated is a $^{12}C^{4+}$ beam with $E_k = 8.77$ keV and chosen emittance values of $\mathcal{E}_x = 63.00\pi$ mm mrad and $\mathcal{E}_y = 54.50\pi$ mm mrad. Quadrupole scan was applied and the beam widths were calculated. For x direction measurements, quadrupole Q5 was kept constant at 28.3 A, while quadrupole Q6 was varied between (23.95 - 41.16) A. Then for y direction measurements, quadrupole Q6 was kept constant at 15.34 A, while quadrupole Q5 was varied between (29.38 - 33.69) A. The quadrupole currents and their respective beam widths obtained are shown in table A.1. It must be noted that the arrangement of data in a table resembles the way it is organized in a text file. The parabolic relation between beam widths and quadrupole currents was observed as shown in figure 5.1. This relation show that the beam is being focused to its minimum waist before being defocused. These obtained beam widths along with their associated magnets currents as well as beam parameters were used to calculate the transverse beam emittance on the emittance calculator. The calculated transverse beam emittance were $\mathcal{E}_x = 63.05\pi$ mm mrad and $\mathcal{E}_y = 54.41\pi$ mm mrad. A complete GUI of the emittance calculator with all required values and the calculated emittances is shown in figure 5.2. Also shown in the figure are the associated ellipses in both transverse directions. Comparing the injected transverse beam emittances with the ones obtained from the emittance calculator it is clear that the injected emittances could be reproduced.

A similar approach was adopted in validating the emittance calculator using the solenoid scan method. A $^1H^{1+}$ beam with $E_k = 9.81$ keV and user defined transverse beam emittance values of $\mathcal{E}_x = 55.40\pi$ mm mrad and $\mathcal{E}_y = 56.30\pi$ mm mrad was injected into TRANSPORT. For the first measurements, solenoid L4Q was kept constant at 17.26 A while solenoid L5Q was altered from (14.8 - 22.8) A. Then for the last five, solenoid L4Q was kept constant at 15.54 A while solenoid L5Q was varied between (15.54 - 22.40) A. The obtained widths together

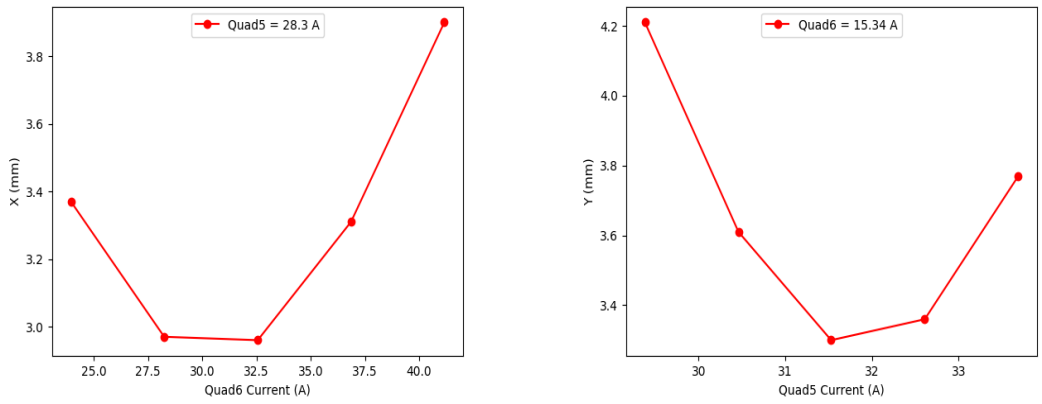

(a) (b)

Figure 5.1: Beam width as function of quadrupole current for $^{12}C^{4+}$ beam; a) horizontal direction and b) vertical direction.

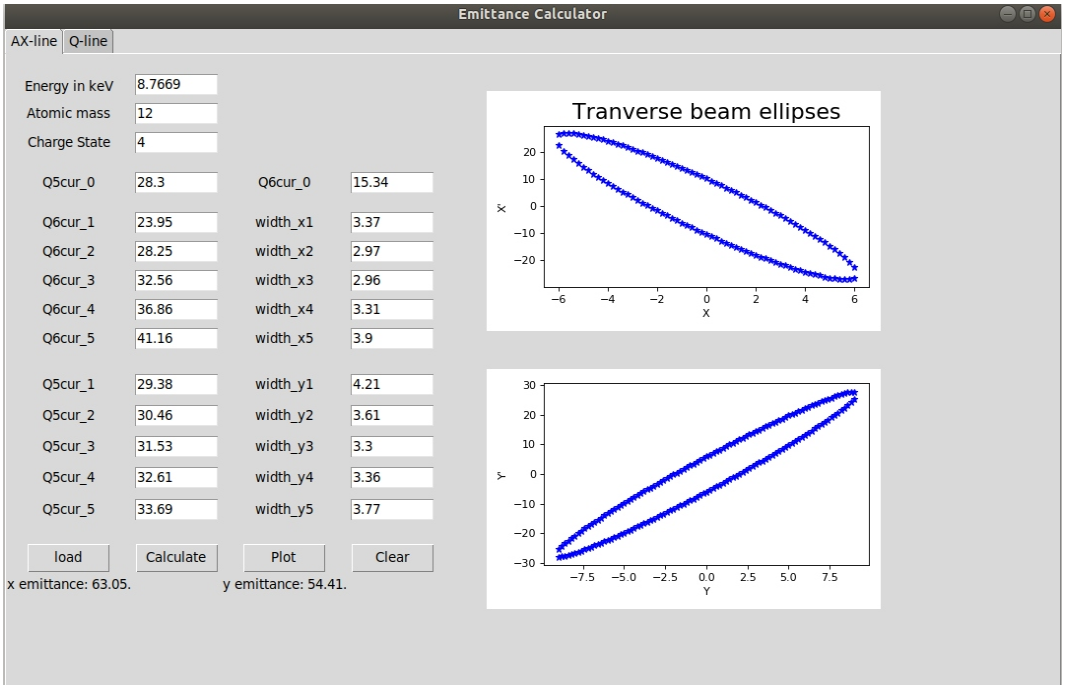

Figure 5.2: Transverse beam emittance calculation done in the AX-line when the $^{12}C^{4+}$ beam was injected on TRANSPORT code for measurements. The two plots show the orientation of the ellipses on each transverse space.

with associated solenoids currents are shown in table A.2. Shown in figure 5.3 are the plots of solenoid currents vs beam widths. The collected data was then accordingly used in the emittance calculator and the calculated transverse beam emittance values were $\mathcal{E}_x = 55.51\pi$ mm mrad and $\mathcal{E}_y = 56.36\pi$ mm mrad as shown in figure 5.4. The associated ellipses in both transverse directions are also shown in the figure. Comparing the injected transverse beam emittances with the calculated ones, it is clear that the results are in agreement.

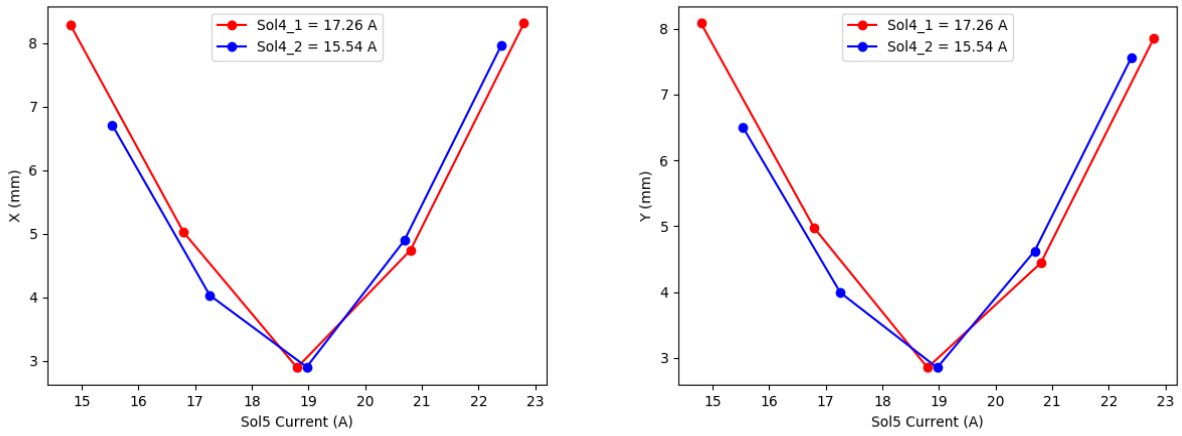

(a) (b)

Figure 5.3: Beam width as function of solenoid current for H^{1+} beam; a) horizontal direction and b) vertical direction.

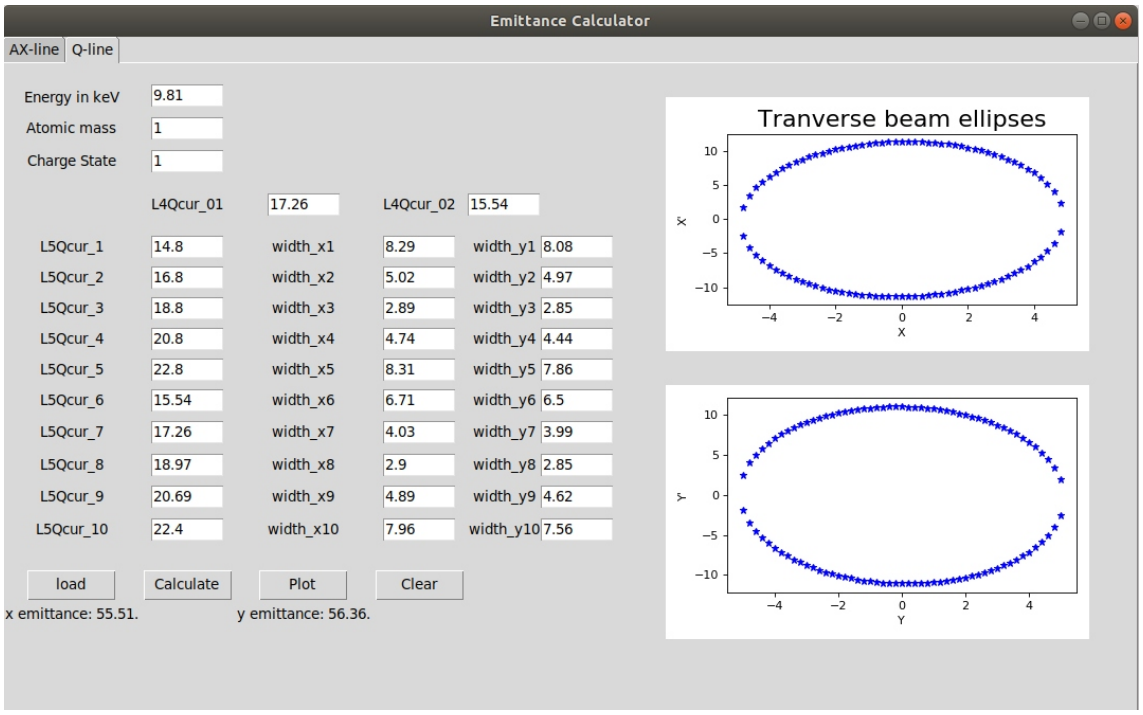

Figure 5.4: Transverse beam emittance calculation done in the Q-line when the $^{1}H^{1+}$ beam was injected into TRANSPORT code for measurements. The two plots show the orientation of the ellipses on each transverse space.

The benchmarking process was also performed using several other different beams. Tables 5.1 and 5.2 show all the beams that were tested with the injected and calculated emittances for both transverse directions shown for both quadruople and solenoid scan. There is clear agreement between injected and calculated emittances. With the benchmarking of the developed system successfully performed, it was decided that the emittance calculator could be tested with real beam measurements.

Table 5.1: The different types of beams with estimated emittance values and E_k, that were injected into the TRANSPORT code in validating quadrupole scan component on the emittance calculator.

Ion	E_k (keV)	Injected		Calculated	
		$\mathcal{E}_x$ (π mm mrad)	$\mathcal{E}_y$ (π mm mrad)	$\mathcal{E}_x$ (π mm mrad)	$\mathcal{E}_y$ (π mm mrad)
$^{12}C^{4+}$	8.767	63.00	54.00	63.02	54.50
$^{20}Ne^{3+}$	13.37	75.60	64.80	76.94	66.50
$^{16}O^{2+}$	15.50	75.00	65.00	75.29	64.84
$^{129}Xe^{6+}$	20.00	85.00	100.0	85.11	99.94
$^{4}He^{1+}$	6.40	100.0	120.0	100.11	120.1
$^{1}H^{1+}$	9.81	55.00	56.00	57.27	55.56

Table 5.2: The different types of beams with estimated emittance values and E_k, that were injected into TRANSPORT in validating solenoid scan component on the emittance calculator.

Ion	E_k (keV)	Injected		Calculated	
		$\mathcal{E}_x$ (π mm mrad)	$\mathcal{E}_y$ (π mm mrad)	$\mathcal{E}_x$ (π mm mrad)	$\mathcal{E}_y$ (π mm mrad)
$^{12}C^{4+}$	8.767	63.00	54.00	63.64	54.43
$^{20}Ne^{3+}$	13.37	75.60	64.80	76.42	60.70
$^{16}O^{2+}$	15.50	75.00	65.00	76.86	63.80
$^{129}Xe^{6+}$	20.00	85.00	100.0	86.36	98.82
$^{4}He^{1+}$	6.040	100.0	120.0	100.6	119.4
$^{1}H^{1+}$	9.81	55.00	56.00	55.51	56.36

5.2 Measurements Results

In the measurements presented below, the GTS ion source at iThemba LABS was used for the generation of ion beams and it was operated at optimum level. Before the measurements are performed, the beam is first tuned properly in the beamline. The beam stability is checked using Faraday cups 3Q, 5Q, 1AX and 2AX. This is to make sure that the measurements in the two beamlines are being performed under similar conditions. The beam profiles are monitored using harps 5Q and 2AX. The two monitors are used to examine if the beam is focused. To focus the beam, the magnets are adjusted accordingly until minimum beam waist is achieved.

Due to the fact that the quadrupole scan is a well understood technique which has been widely used, it was decided that when performing the measurements one needs to start with this method in the AX-line before proceeding with the solenoid scan in the Q-line. This is to make sure that if there is something wrong with the beam being extracted it will be easier to diagnose using the qudrupole scan. In performing the measurements, the minimum beam waist is found then the beam widths are gathered while changing the strength of quadrupoles Q5 and Q6 in the AX-line. If the quadrupole scan procedure is successful, then the solenoid scan will subsequently follow. The similar approach is adopted for solenoid scan, solenoids L4Q and L5Q are changed accordingly. Then beam widths are gathered. The measurements reported in this work were performed using helium and silicon beams.

5.2.1 Helium Measurements

Using the automated Bash script developed, the first beam width measurements were performed using quadrupole scan method with $^4He^{2+}$ beam having E_k = 12.70 keV. The beam current measured with Faraday cup 2AX was approximately 41.0 μA and it was stable. For x direction measurements, quadrupole Q5 was kept constant at 26.80 A while quadrupole Q6 was varied from (19.0 - 27.0) A and the beam widths were recorded. Then, for y direction measurements, quadrupole Q6 was kept constant at 18.00 A while quadrupole Q5 was varied from (24.9 - 27.3) A and the beam widths were also recorded. The data in table A.3 shows the quadrupole currents alongside the beam widths gathered. Figure 5.5 shows the relation between quadrupole currents and the beam widths. The calculated beam emittances obtained for these measurements were $\mathcal{E}_{x,rms}$ = 33.30±0.003π mm mrad* and $\mathcal{E}_{y,rms}$ = 26.72±0.001π mm mrad and can be seen in figure 5.6. Also shown are the associated beam ellipses for both transverse spaces.

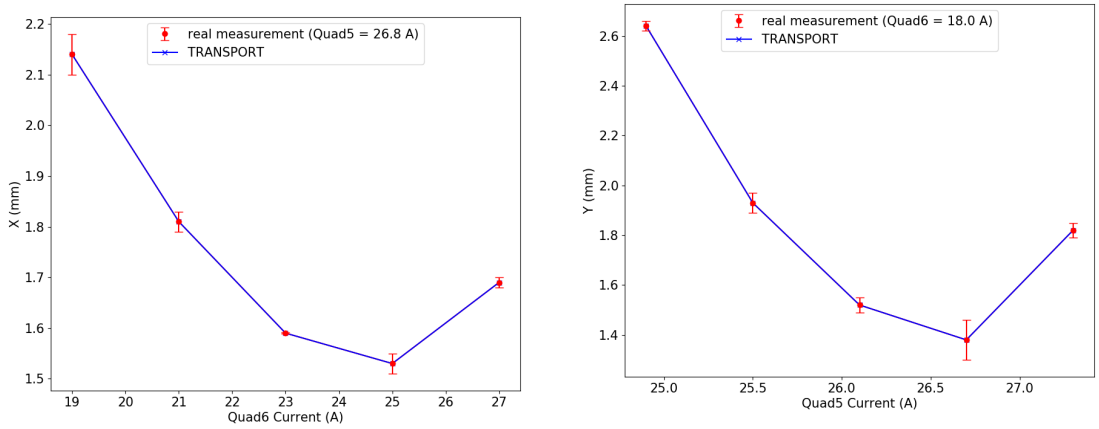

(a) (b)

S

Figure 5.5: Beam width as function of quadrupole current for $^4He^{2+}$ beam; a) horizontal direction and b) vertical direction.

With the same $^4He^{2+}$ beam, the measurements were performed in the Q-line. The beam current measured with Faraday cup 5Q was approximately 42.0 μA and the stability was acceptable. By following solenoid scan method, for the first five measurements taken, solenoid

*Method used to propagated errors can be found in Appendix B.

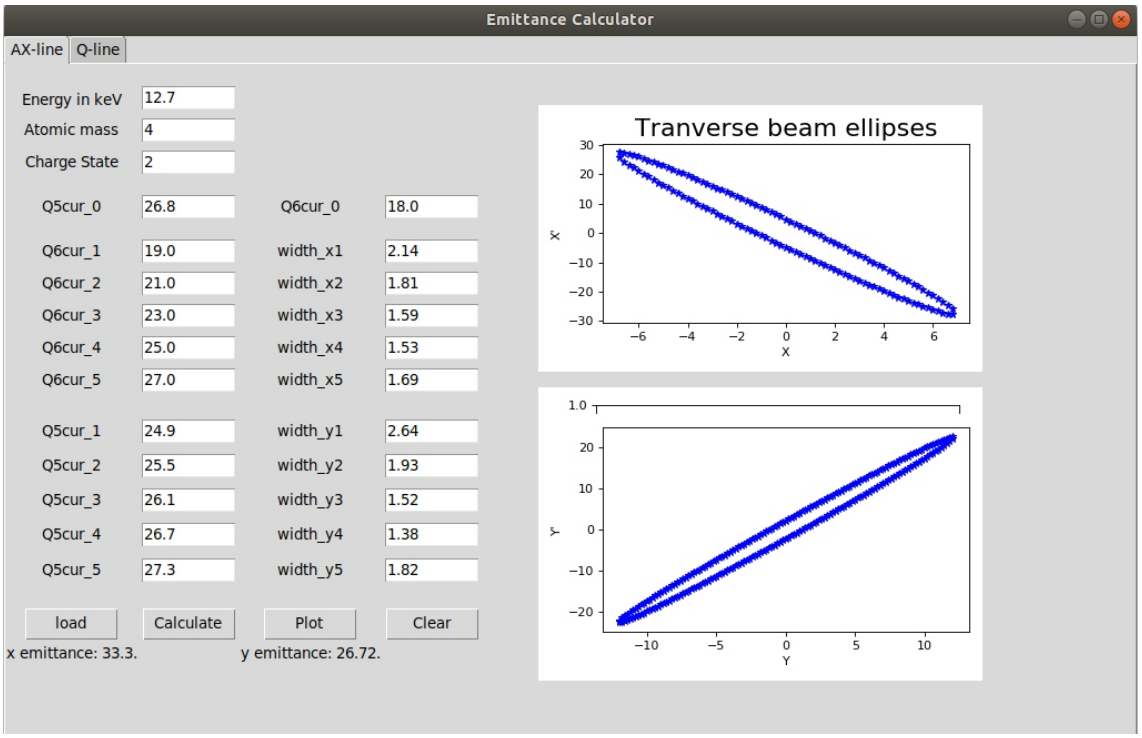

Figure 5.6: Transverse beam emittance calculation done in the AX-line when the real $^4He^{2+}$ beam was used for measurements. The two plots show the orientation of the ellipses on each transverse space.

L4Q was kept constant at 40.02 A while solenoid L5Q was altered from (29.3 - 35.7) A. Then for the last five, solenoid L4Q was changed and kept constant at 37.02 A while solenoid L5Q was altered again from (29.3 - 35.7) A. The beam widths obtained are shown in table A.4 and the solenoid currents against beam widths plots are depicted in figure 5.7. Also the measured beam widths and associated solenoid currents, particles mass, charge state and kinetic energy were used to calculate transverse beam emittance. The calculated beam emittances were $\mathcal{E}_{x,rms} = 137.18 \pm 0.01\pi$ mm mrad and $\mathcal{E}_{y,rms} = 59.66 \pm 0.06\pi$ mm mrad as shown in figure 5.8. Also shown are the associated beam ellipses for both transverse spaces.

When one looks at the the obtained transverse beam emittances above, it is clear that there is a discrepancy between emittance measured in the AX-line and measured in the Q-line. The emittances obtained in the Q-line are very much larger than that obtained for AX-line. According to the Liouville's theorem which states that, if there are no external forces acting on the particles (beam) the density/volume of particles in phase space between two points remains invariant. This

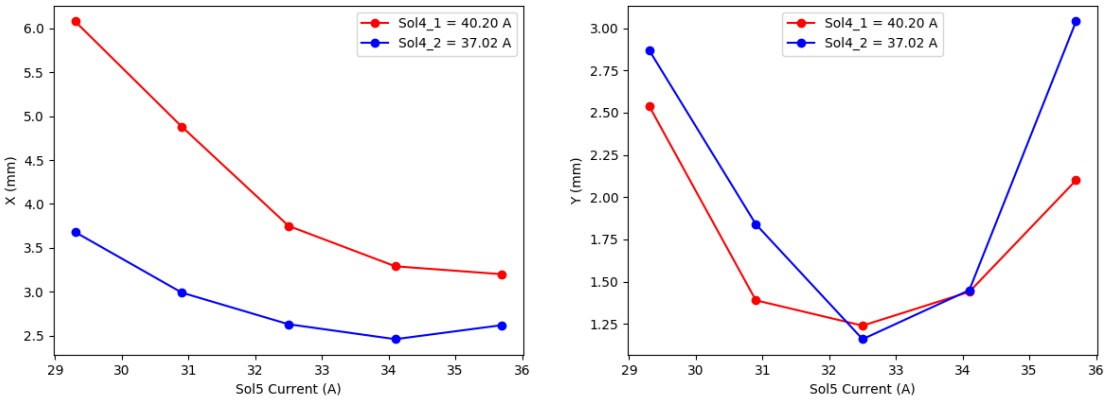

(a) (b)

Figure 5.7: Beam width as function of solenoid current for $^4He^{2+}$ beam; a) horizontal direction and b) vertical direction.

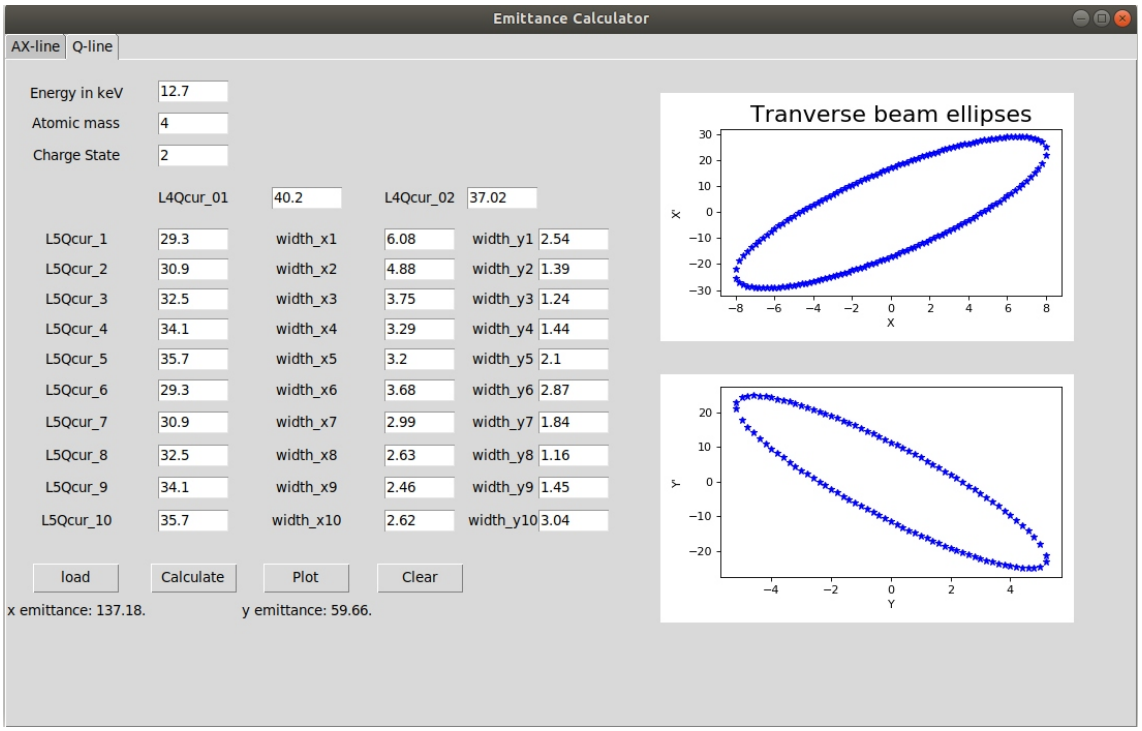

Figure 5.8: The transverse beam emittance results from calculations for Q-line when the actual $^4He^{2+}$ beam was used for measurements. The two plots show the orientation of the ellipses on each transverse space.

means that in our case the beam emittances measured in the Q-line and AX-line should remain the same. This must be true if there are no external forces acting on the beam. Looking at the beam currents measured with Faraday cup 2AX and 5Q it is clear that the is no beam current reduction between the two points. So one can conclude that the density remain invariant. However, the emittance results have significant disagreement, which suggest that the Liouville theorem is violated. In order to investigate the source of this emittances disagreement it was decided that a second set of measurements must be performed. Now, because a number of measurements had been performed already using the helium beam and the resulted emittances had discrepancies, it only made sense to use a different beam for further investigations. Therefore a silicon beam was randomly chosen.

5.2.2 Silicon Measurements

The second set of measurements were performed using the $^{32}Si^{5+}$ beam with $E_k = 8.35$ keV. The beam current measured in Faraday cup 2AX was approximately 14.0 μA and the beam was stable. By following quadrupole scan approach described in section 4.2, quadrupole Q5 was kept constant at 34.25 A while varying quadrupole Q6 from (23.5 - 33.5) A and the horizontal beam widths were recorded. Then for vertical direction, the quadrupole Q6 was kept constant at 22.50 A while varying quadrupole Q5 from (32.65 - 35.85) A and collecting the associated vertical beam widths. The results in table A.5 shows the quadrupole currents with the associated beam widths obtained. Figure 5.9 shows the plots of quadrupole currents vs beam widths. The calculated beam emittances obtained in this case were $\mathcal{E}_{x,rms} = 40.58 \pm 0.04\pi$ mm mrad and $\mathcal{E}_{y,rms} = 69.14 \pm 0.03\pi$ mm mrad as shown in figure 5.10. Also shown are the beam ellipses for both transverse spaces.

Using the same beam, the measurements were performed in the Q-line. The recorded beam current was approximately 16.0 μA and the beam was stable. For the first five measurements solenoid L4Q was kept constant at 43.75 A while varying solenoid L5Q from (38.15 - 44.55) A to obtain and record the both sets of beam widths. Then for the last five measurements solenoid L4Q was changed to 43.95 A

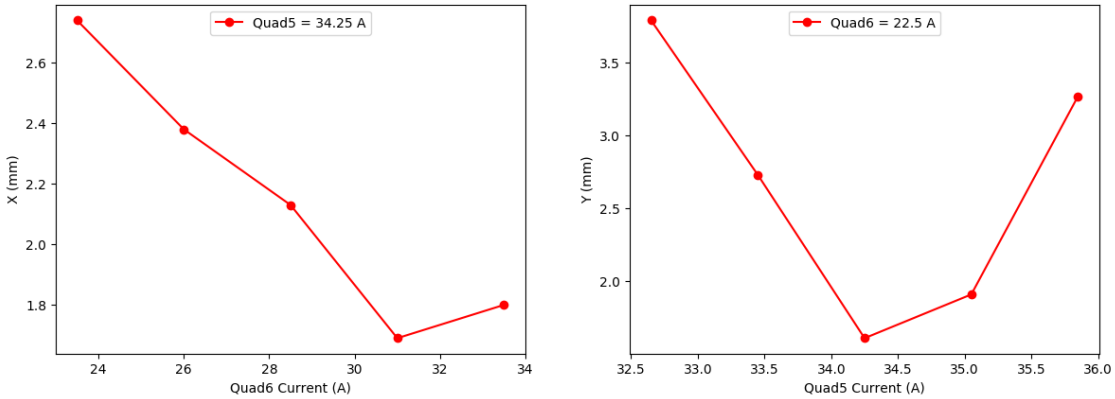

(a) (b)

Figure 5.9: Beam width as function of quadrupole current for $^{32}Si^{5+}$ beam; a) horizontal direction and b) vertical direction.

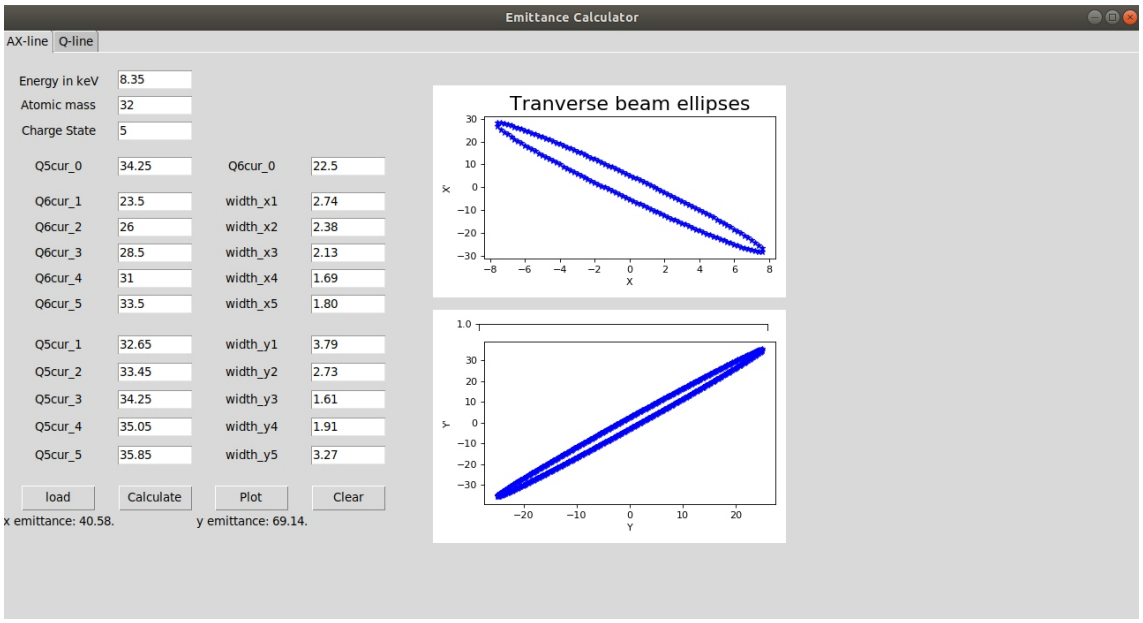

Figure 5.10: Transverse beam emittance calculation done in the AX-line when the real $^{32}Si^{5+}$ beam was used for measurements. The two plots show the orientation of the ellipses on each transverse space.

while solenoid L5Q was altered from (37.55 - 43.95) A. The beam widths obtained are shown in table A.6 and the solenoid currents against widths plots are depicted in figure 5.11. Also, the measured widths and associated solenoid currents, particles mass, charge state and kinetic energy were used to calculate transverse beam emittance. The calculated beam emittances were $\mathcal{E}_{x,rms} = 121.70 \pm 0.43\pi$ mm mrad and $\mathcal{E}_{y,rms} = 156.07 \pm 0.43\pi$ mm mrad as shown in figure 5.12. Also shown are the associated beam ellipses for both transverse spaces.

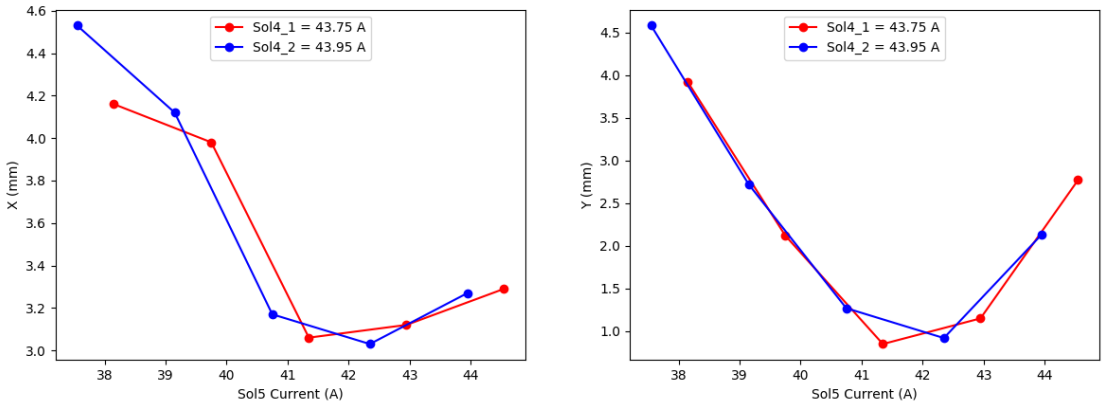

(a) (b)

Figure 5.11: Beam width as function of solenoid current for $^{32}Si^{5+}$ beam; a) horizontal direction and b) vertical direction.

The obtained beam emittances above also show a trend that was observed in the helium measurement. There is still discrepancy between beam emittances obtained in the AX-line and the ones obtained in the Q-line. The obtained emittances in the Q-line are higher than those from AX-line. These observations remain an misunderstood and unresolved mystery. Since this tendency could be reproduced in the two measurements, it is clear that this tendency is unrelated to the the beam but could be due to the way measurements are being performed. In order to understand if there was anything wrong with the way the measurements are being performed it was decided that the beam widths measured should be simulated with TRANSPORT.

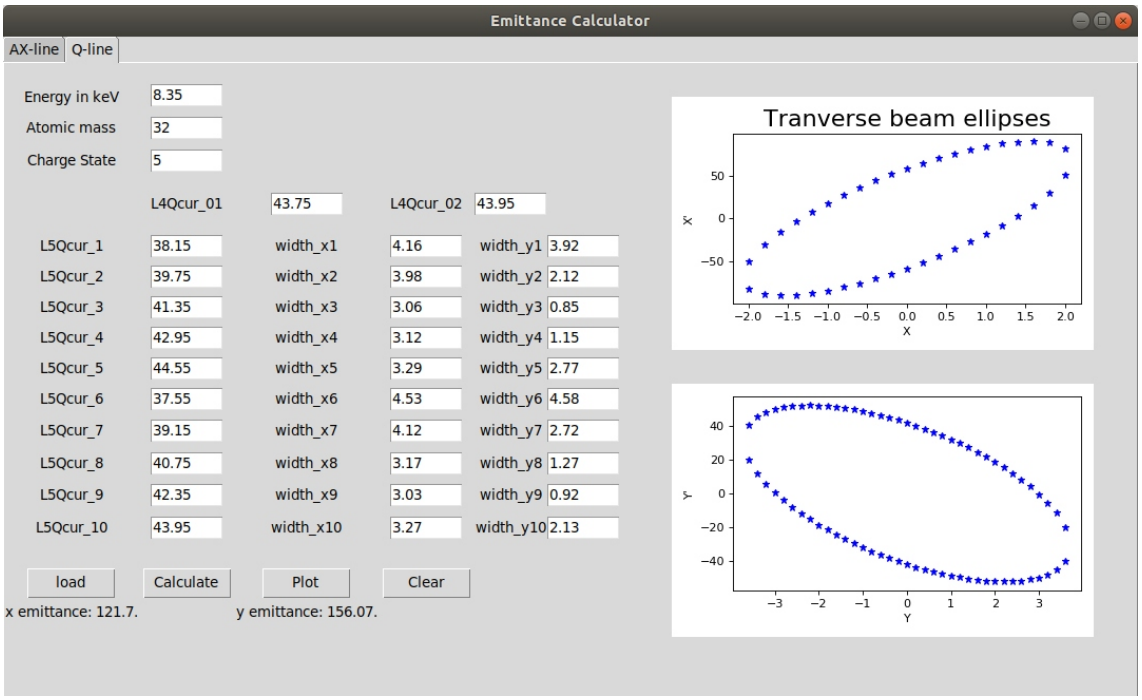

Figure 5.12: Transverse beam emittance calculation done in the Q-line when the real $^{32}Si^{5+}$ beam was used for measurements. The two plots show the orientation of the ellipses on each transverse space.

5.3 Beam widths Comparison

In order to investigate the source of disagreement between the emittances in two the beamlines, the helium beam was used. The measured widths and the beam widths simulated using TRANSPORT were compared. Firstly the obtained beam emittances from the AX-line measurement were injected into TRANSPORT. The quadrupole scan was performed using the quadrupole settings similar to the ones used during the measurements. The same approach of gathering beam widths was also adopted when using TRANSPORT. Both sets of widths were then compared with each other. Figure 5.13 shows the two plots of beam widths against quadrupole currents for both widths obtained from TRANSPORT and the measured widths. The red data points indicate beam widths acquired from measurements and the blue line shows beam widths obtained from TRANSPORT. When one compares simulated and measured widths it is visible that they follow similar trend.

In order to probe how the Q-line beam widths compare with the ones obtained from TRANSPORT, the obtained beam emittances from

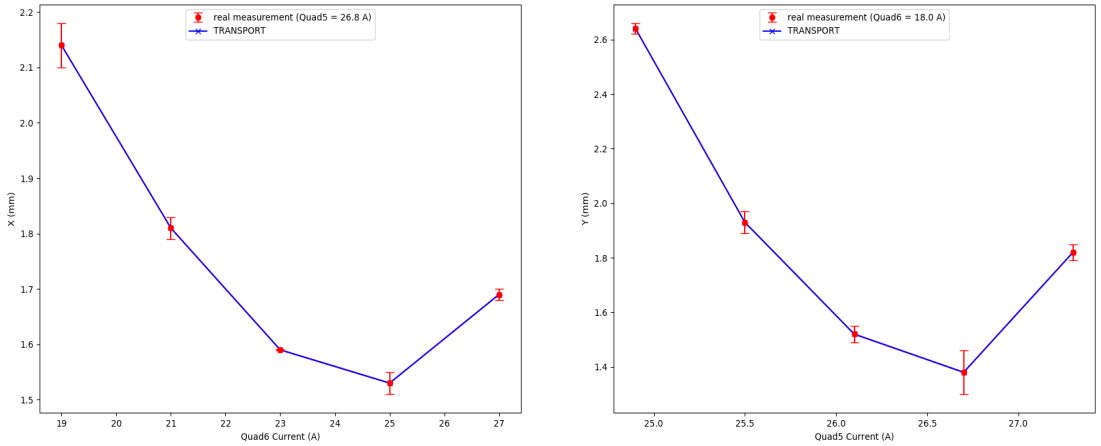

(a) (b)

Figure 5.13: Beam width as function of quadrupole current for $^4He^{2+}$ when beam widths from TRANSPORT and measurements are compared; a) horizontal direction and b) vertical direction.

Q-line measurements were injected into TRANSPORT. The solenoid scan was performed using the same solenoid currents as the ones used during measurements and similar approach of gathering beam widths was followed. The beam widths were obtained using TRANSPORT and they were compared with the ones gathered during measurements. Figure 5.14 shows four plots of measured and simulated beam widths versus solenoid currents. Figures 5.14a and 5.14b shows beam widths taken in a horizontal direction and figures 5.14c and 5.14d are beam widths taken for a vertical direction. The blue lines indicate beam widths obtained from TRANSPORT and grey lines with red data points are widths gathered from measurements. From these figures it is clear that there is obvious disagreement between widths obtained from TRANSPORT and the measured widths.

By looking at the beam widths comparison performed above, it is visible that the beam widths measured in the AX-line could be easily reproduced using TRANSPORT. On the other hand, when one compare the measured beam widths obtained in the Q-line with the simulated widths there seems to be very clear disagreement between them. These observations indicate that the emittances obtained in the Q-line couldn't be relied on. It was now obvious that something unexpected was happening in this beamline.

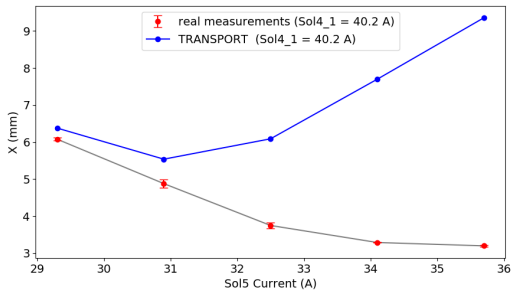

(a) first five widths in a horizontal direction

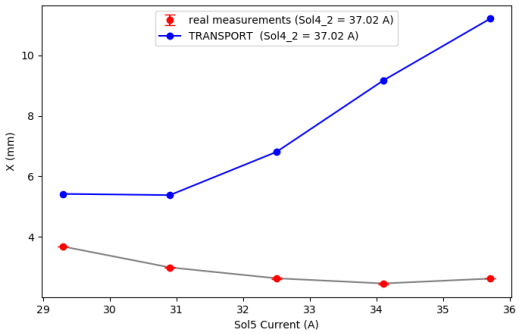

(b) last five widths in a horizontal direction

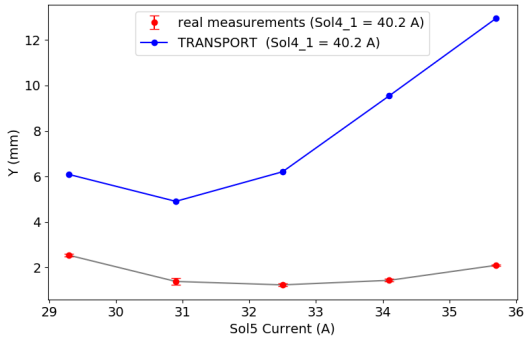

(c) first five widths in the vertical direction

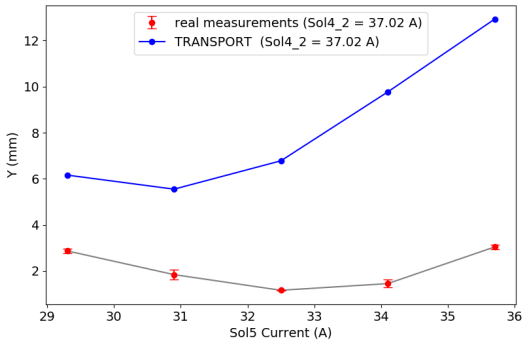

(d) last five widths in the vertical direction

Figure 5.14: Beam width as function of solenoid current for $^4He^{2+}$ beam when widths from TRANSPORT and measurements are compared.

5.4 Discussion

Through the benchmarking process the emittance calculator showed that it was working as expected. The benchmarking process was achieved by attempting to reproduce known emittances which were injected into TRANSPORT. The injected emittances could be reproduced with the emittance calculator. However, when the emittance calculator was used to deduce the measured emittances with real beams it was found that the results obtained in the AX-line and the ones from Q-line are in disagreement. The emittances obtained in the Q-line were much larger than those obtained in the AX-line. The results were unexpected as it is assumed that the emittances obtained in the two beamlines must remain the same. In probing for the source of disagreement in the results, the second measurements were performed. The results from the second set of measurements also depicted the same discrepancy observed in the first set of measurements. In order to further investigate the source of discrepancy between the two beamlines, the measured widths were compared with the simulated beam widths. The widths were simulated by injecting the obtained emittances into TRANSPORT. This was done for helium measurements. From the comparisons it was observed that the beam widths measured in the AX-line could be reproduced using TRANSPORT. On the other hand, the measured beam widths measured in the Q-line showed a clear disagreement with the ones from TRANSPORT. From these observations it was evident that there was something unexpected going in the Q-line.

When looking closely to the Q-line, it was noticed that errors on beam widths affect the deduced emittances. This was checked by increasing and decreasing gathered beam width(s) by 0.1 mm for both silicon and helium measurements. For AX-line measurements one beam width was increased and decreased by 0.1 mm and the emittance was deduced. The deduced emittances were compared with the original ones and the results are depicted in table 5.3. For Q-line measurements one beam width on each direction was increased and decreased by 0.1 mm simultaneously and the emittances were deduced. The deduced emittances were then compared with the original ones and the results are depicted in table 5.4.

From the emittance comparison tables, for AX-line measurements it is visible that when one gathered beam width has an error, it does not affect the emittance largely. On the other hand for Q-line measurements when one gathered beam width has an error, the emittance is affected largely. This made AX-line measurements more reliable and also gave an idea of what could be the source of the discrepancy.

For a quadrupole scan utilized in the AX-line, a minimum of three measurements are required to determine the emittance but in this case five measurements were used. This choice of number of measurements proved to be a good choice as it reduced the effect of errors on the overall emittance. Then for solenoid scan which is utilized in the Q-line, a minimum of ten measurements are required to determine emittance and in this case, that minimum number was used. This made the system to be prone to errors hence the determined emittances were affected largely.

Table 5.3: Comparison of calculated transverse beam emittances between helium and silicon measurements in the AX-line when one measured beam width on both x and y directions were altered by 0.1 mm up and down.

	Helium measurements			Silicon measurements		
	Original	0.1 mm ↑	0.1 mm ↓	Original	0.1 mm ↑	0.1 mm ↓
$\mathcal{E}_{x,rms}$ (π mm mrad)	33.30	32.24	34.10	40.58	34.74	44.93
$\mathcal{E}_{y,rms}$ (π mm mrad)	26.72	27.46	25.87	69.14	70.45	67.83

Table 5.4: Comparison of calculated transverse emittances between helium and silicon measurements in the Q-line when one measured beam widths in x and y directions were simultaneously altered by 0.1 mm up and down.

	Helium measurements			Silicon measurements		
	Original	0.1 mm ↑	0.1 mm ↓	Original	0.1 mm ↑	0.1 mm ↓
$\mathcal{E}_{x,rms}$ (π mm mrad)	137.18	140.26	134.05	121.70	155.01	75.27
$\mathcal{E}_{y,rms}$ (π mm mrad)	59.66	61.80	57.34	156.07	170.46	141.04

Another task that was looked into was emittance swapping. This was done in order to check if it still holds since the beamline was last modified. As previously mentioned in chapter 2, solenoids (L2Q-L5Q) together with the decommissioned ECRIS in the LEBT were designed in such a way that if all solenoids have the same current

settings and their polarity are applied accordingly, the transverse beam emittance from the source will swap before injected into the AX-line. This means that if the beam extracted from the source with $\mathcal{E}_x$ = a and $\mathcal{E}_y$ = b these emittances will be swapped before injected into the AX-line i.e the emittances measured in the AX-line will be $\mathcal{E}_x$ = b and $\mathcal{E}_y$ = a. However, the GTS ion source is connected to the LEBT differently from the previous ECRIS. By looking at the obtained beam emittances, it is impossible to conclude if the emittance swapping is achieved since the results from the Q-line were unreliable.

Chapter 6

Conclusions and Outlook

6.1 Conclusion

The primary objective for this research project was to develop a system that will assist the ECRIS users in determining transverse beam emittances in the LEBT leading to SPC2. An analytical model was developed which allows the determination of transverse beam emittances from beam profile measurements. The model is based on matrix formalism and was developed using Python programming language. Two methods of emittance measurement were used namely; quadrupole scan and solenoid scan. Quadrupole scan utilized in the AX-line was achieved by using quadrupoles Q5 and Q6 in the AX-line, where Q6 was varied to gather beam widths in the x direction and Q5 was varied to gather beam widths in the y direction. Solenoid scan in the Q-line was achieved by using the last two solenoids L4Q and L5Q. This was done by keeping solenoid L4Q constant while varying solenoid L5Q in order to gather beam widths in both x and y directions for the first five measurements. Then for the last five measurements, solenoid L4Q current was changed and kept constant and solenoid L5Q current was varied five times while also gathering beam widths in both x and y directions.

This newly developed emittance calculator was validated using TRANSPORT. Different types of beams with user defined transverse emittances were injected into TRANSPORT. The solenoid scan and quadrupole scan were subsequently used to gather beam widths in both directions. The gathered beam widths along with the associated magnets currents as well as beam parameters were used in the emittance

calculator to compute the emittances. By comparing the injected emittances and the calculated ones, it was found that there was an agreement. This meant that the emittance calculator was working appropriately. The next step was to perform measurements.

A Gaussian approximation program was developed using Bash scripting, C++ and EPICS. The program was used to get beam widths of the beam profile from profile monitors. The first beam width measurements were performed using a $^4He^{2+}$ beam and the obtained beam emittances after doing the calculations for AX-line were $\mathcal{E}_{x,rms} = 33.30\pm0.003\pi$ mm mrad and $\mathcal{E}_{y,rms} = 26.72\pm0.0001\pi$ mm mrad while for Q-line $\mathcal{E}_{x,rms} = 137.18\pm0.01\pi$ mm mrad and $\mathcal{E}_{y,rms} = 59.66\pm0.06\pi$ mm mrad. These results showed discrepancy between the obtained transverse beam emittances in the AX-line and Q-line. The emttances obtained in the Q-line were much higher than the ones obtained in the AX-line. Further investigations were performed by doing another measurement. The emittance measurements were performed using $^{32}Si^{5+}$ beam. The obtained beam emittances were $\mathcal{E}_{x,rms} = 40.58\pm0.01\pi$ mm mrad and $\mathcal{E}_{y,rms} = 69.14\pm0.06\pi$ mm mrad in the AX-line and $\mathcal{E}_{x,rms} = 121.70\pm0.43\pi$ mm mrad and $\mathcal{E}_{y,rms} = 156.07\pm0.43\pi$ mm mrad in the Q-line. The results obtained in the second measurement also showed discrepancy between the obtained transverse beam emittances.

Further probing was done whereby beam widths from helium measurements were compared with TRANSPORT simulated widths. From this task the measured beam widths in the AX-line were comparable with the ones obtained from TRANSPORT for this beamline. However, for Q-line there was a large disagreement between the measured and simulated widths. From these observations it was clear that when one is using the newly developed emittance calculator they could rely more on beam emittances obtained from the AX-line with those obtained from Q-line being less reliable. This indicated that there was something unexpected happening when deducing emittances in the Q-line beamline.

When performing any kind of measurements it is a known fact that the results obtained will have errors associated with them. This also applies to the widths measurements performed in the current work. In attempting to see how errors on beam widths would affect the obtained emittances one of the widths obtained was increased and

decreased by 0.1 mm on each direction and the emittances were recalculated. From the observations it was clear that when one changes the widths in the AX-line not much change was observed in the obtained emittances. Whereas this was not the case in the Q-line beamline. The change in widths in the Q-line resulted in drastic reduction or increase in emittances. The reason behind this could be associated with the number of measurements required to deduce the emittances. For AX-line measurements one need a minimum of three widths measurements to deduce emittances and in the current work five measurements were utilized. This choice of number measurements is believed to have made the AX-line measurements to be tolerant to errors. For Q-line measurements however, only the minimum number of measurements (ten) were utilized. This makes the measurements in this beamline to be prone to errors. Therefore for much more reliable emittance measurements in the Q-line the number of measurements utilized have to be increased. This need to be augmented in the next version of the emittance calculator.

6.2 Outlook

From the results presented in this work, the transverse beam emittances measured between Q-line and AX-line had discrepancies. These discrepancies could be due to error(s) on beam widths measurements affecting the deduced emittances largely for the Q-line. Therefore in fixing this, the number of beam widths required to determine beam emittances when using solenoid scan technique have to increase. In increasing the number of measurements, it should be taken into account that the beam profile in the harps might overshoots. Therefore a strategic approach is needed in order to overcome this challenge.

On the next version of emittance calculator, the emittance in 4D will be included as it holds true for Liouville theorem. So, emittance in 4D measured in Q-line must be the same as the one measured in AX-line. Investigation on whether the emittance swapping still holds will be undertaken. Since the emittances deduced in the AX-line are reliable, this version of emittance calculator can be used in future to do the following tasks:

- Use these transverse emittances as diagnostic tool to improve beam quality.
- It is now possible to investigate the SPC2 cyclotron acceptance which can be used for matching the LEBT with the cyclotron for better beam transmission.
- The input files for most beam simulations can now be populated with realistic emittance parameters.
- Investigation of how source parameters i.e magnetic confinement, frequency, charge state and ion temperature affect extracted emittances from GTS ion source.
- The contribution of plasma stability on emittance can also be probed.
- The influence of ion beam intensity on emittance.
- Establishing and modelling of the initial conditions of charge particle beams at extraction aperture.

All these tasks mentioned above will allow the researchers in the ion source division to better their understanding of the ECR sources. Hence, the improvements in the operation of the GTS source can be anticipated.

Appendix A

Tables Of Beam Widths Alongside Magnets Currents

A.1 TRANSPORT Calculations

The following tables A.1 and A.2 show focusing currents along with beam widths calculated from TRANSPORT code by injecting estimated emittances using $^{12}C^{2+}$ beam with $E_k = 8.77$ keV and $^{1}H^{1+}$ beam with $E_k = 9.81$ keV. The estimated emittance values for these beams were $\mathcal{E}_x = 63.00\pi$mm mrad & $\mathcal{E}_y = 54.00\pi$ and $\mathcal{E}_x = 55.40\pi$mm mrad & $\mathcal{E}_y = 56.70\pi$mm mrad for carbon and hydrogen beams respectively.

Table A.1: The calculated beam widths with the associated quadrupole currents using $^{12}C^{2+}$ beam injected into TRANSPORT.

Q6 (A)	Q5 (A)	x (mm)	Q6 (A)	Q5 (A)	y (mm)
23.95	28.3	3.37	15.34	29.38	4.21
28.25	28.3	2.97	15.34	30.46	3.61
32.56	28.3	2.96	15.34	31.53	3.30
36.86	28.3	3.31	15.34	32.61	3.36
41.16	28.3	3.90	15.34	33.69	3.77

Table A.2: The calculated beam widths with the associated solenoid currents using $^1H^{1+}$ beam injected into TRANSPORT.

L4Q (A)	L5Q (A)	x (mm)	y (mm)
17.26	14.80	8.29	8.08
17.26	16.80	5.02	4.97
17.26	18.80	2.89	2.85
17.26	20.80	4.74	4.44
17.26	22.80	8.31	7.86
15.54	15.54	6.71	6.50
15.54	17.26	4.03	3.99
15.54	18.97	2.90	2.85
15.54	20.69	4.89	4.62
15.54	22.4	7.96	7.56

A.2 Real Measurements

The tables from A.3-A.6 show measurement results obtained from performing beam width measurements on the real beams.

Table A.3: Obtained beam widths from measurements with the associated quadrupole currents using $^4He^{2+}$ beam.

Q6(A)	Q5(A)	x(mm)	Q6(A)	Q5(A)	y(mm)
19	26.8	2.14	18	24.9	2.64
21	26.8	1.81	18	25.5	1.93
23	26.8	1.59	18	26.1	1.52
25	26.8	1.53	18	26.7	1.38
27	26.8	1.69	18	27.3	1.82

Table A.4: Obtained beam widths from measurements with the associated solenoid currents using $^4He^{4+}$ beam.

L4Q(A)	L5Q(A)	x(mm)	y(mm)
40.2	29.3	6.08	2.54
40.2	30.9	4.88	1.39
40.2	32.5	3.75	1.24
40.2	34.1	3.29	1.44
40.2	35.7	3.20	2.10
37.02	29.3	3.68	2.87
37.02	30.9	2.99	1.84
37.02	32.5	2.63	1.16
37.02	34.1	2.46	1.45
37.02	35.7	2.62	3.04

Table A.5: Obtained beam widths from measurements with the associated quadrupole currents using $^{32}Si^{5+}$ beam.

Q6(A)	Q5(A)	x(mm)	Q6(A)	Q5(A)	y(mm)
23.5	34.25	2.74	22.5	32.65	3.79
26.0	34.25	2.38	22.5	33.45	2.73
28.5	34.25	2.13	22.5	34.25	1.61
31.0	34.25	1.69	22.5	35.05	1.91
33.5	34.25	1.80	22.5	35.85	3.27

Table A.6: Obtained beam widths from measurements with the associated solenoid currents using $^{32}Si^{5+}$ beam.

L4Q(A)	L5Q(A)	x(mm)	y(mm)
43.75	38.15	4.16	3.92
43.75	39.75	3.98	2.12
43.75	41.35	3.06	0.85
43.75	42.95	3.12	1.15
43.75	44.55	3.29	2.77
43.95	37.55	4.53	4.58
43.95	39.55	4.12	2.72
43.95	40.75	3.17	1.27
43.95	42.35	3.03	0.92
43.95	43.95	3.27	2.13

Appendix B

Error Estimation

B.1 The Chi Squared Distribution

For any experimental data, errors are inevitable and the best thing that one can do is to minimize them. In this case a χ^2 test was used to give some insight into the agreement between an observed distribution of measurements and the true distribution, by a sum of squares with the following general Eq. [52].

$$\chi^2 = \sum_{i=1}^{n} \left(\frac{observed\ value - true\ value}{standard\ deviation} \right)^2 \tag{B.1}$$

The observed values are beam widths from measurements performed and true values are the correct beam widths without any error encountered.

Now, given the above Eq.B.1 the best estimates for the $\sigma_x(i)$ are acquired by the following expression

$$\chi^2 = \sum_{i=1}^{n} \left(\frac{\sigma_x(i) - (R_{11}^2(i)\sigma_{11}^0 + 2R_{11}(i)R_{12}(i)\sigma_{12}^0 + R_{12}^2(i)\sigma_{22}^0)}{\delta(i)} \right)^2 \tag{B.2}$$

where n is the number of measurements, $\delta(i)$ denotes the error and Rs & σ^0s represent the beam transfer matrix of the expected distribution as well its elements respectively. Furthermore the χ^2 partial derivatives were taken against $\sigma^0(i)$ (see [53])) in order to obtain the

following expression

$$\begin{bmatrix} \sum \frac{R_{11}^2(i)\sigma(i)}{\delta^2(i)} \\ \sum \frac{2R_{11}(i)R_{12}(i)\sigma(i)}{\delta^2(i)} \\ \sum \frac{R_{12}^2(i)\sigma(i)}{\delta^2(i)} \end{bmatrix} = \begin{bmatrix} \sum \frac{R_{11}^4(i)}{\delta^2(i)} & \sum \frac{R_{11}^3 R_{12}(i)}{\delta^2(i)} & \sum \frac{R_{11}^2(i)R_{12}^2}{\delta^2(i)} \\ \sum \frac{2R_{11}^3 R_{12}(i)}{\delta^2(i)} & \sum \frac{4R_{11}^2 R_{12}^2(i)}{\delta^2(i)} & \sum \frac{2R_{11}^2(i)R_{12}^3}{\delta^2(i)} \\ \sum \frac{R_{11}^2 R_{12}^2(i)}{\delta^2(i)} & \sum \frac{2R_{11}R_{12}^3(i)}{\delta^2(i)} & \sum \frac{R_{12}^4(i)}{\delta^2(i)} \end{bmatrix} \begin{bmatrix} \sigma_{11}^0 \\ \sigma_{12}^0 \\ \sigma_{22}^0 \end{bmatrix}. \tag{B.3}$$

The above Eq.B.3 is in the familiar form $\mathbf{Ax} = \mathbf{b}$, where $\mathbf{A}$ is the curvature matrix coefficients and $\mathbf{b}$ is the matrix with the sum of the product of the measured beam widths and the transfer matrix elements. Then, in order to solve for x, an inverse of $\mathbf{A}$ is taken and multiplied by $\mathbf{b}$:

$$x = A^{-1}b. \tag{B.4}$$

The matrix inverse of A is also known as *error matrix* and its elements give the error estimates. Therefore in this case elements (R_{11} and R_{12}) give error estimates.

Figures from B.1 - B.4 show the line(s) of best fit to beam widths measurements. Also depicted are the parabolic relations between focusing currents and gathered beam widths. Then as for errors on beam emittances, Eq.B.3 was used to calculate the true widths and Eq.B.5 to get errors. These anticipated true widths were used to deduce the true emittances. Then the true emittances together with the measured emittances were used to get errors on the measured emittances. The following equation below was used to deduce errors on the measured emittances.

$$\mathcal{E}_{error} = |\mathcal{E}_{measured} - \mathcal{E}_{true}| \tag{B.5}$$

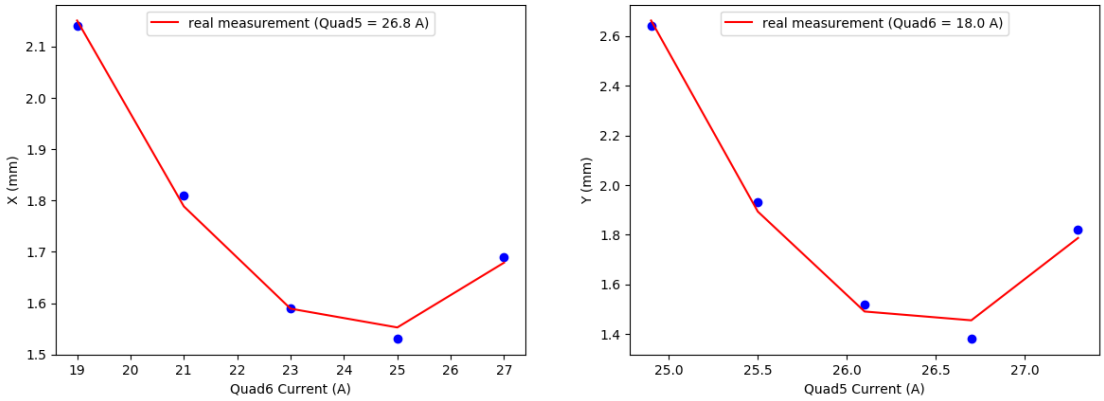

(a) (b)

Figure B.1: Plots showing the best fit of quadrupole currents against the beam widths for $^4He^{2+}$ beam; a) horizontal direction and b) vertical direction.

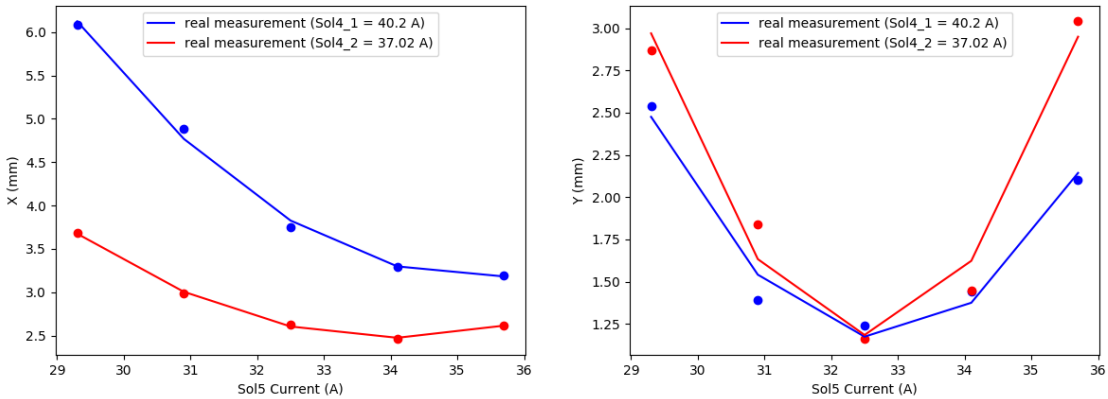

(a) (b)

Figure B.2: Plots showing the best fit of solenoid currents against the beam widths for $^4He^{2+}$ beam; a) horizontal direction and b) vertical direction.

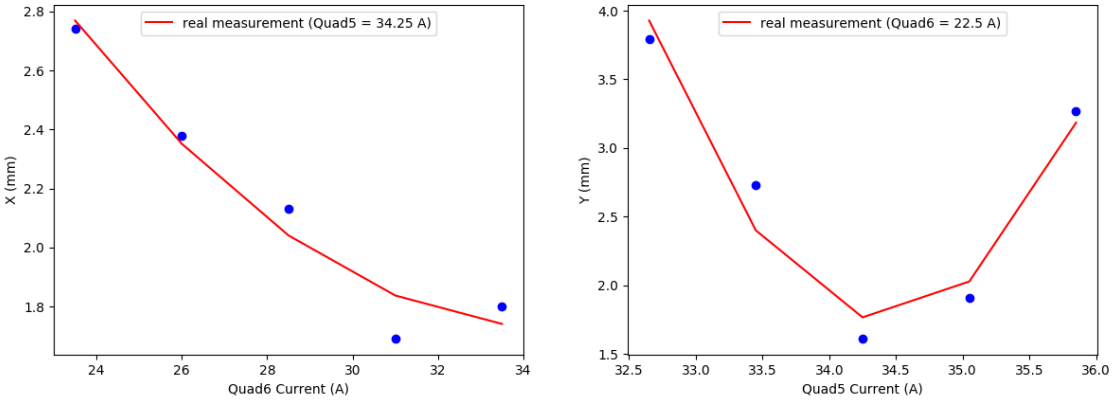

(a) (b)

Figure B.3: Plots showing the best fit of quadrupole currents against the beam widths for $^{32}Si^{5+}$ beam; a) horizontal direction and b) vertical direction.

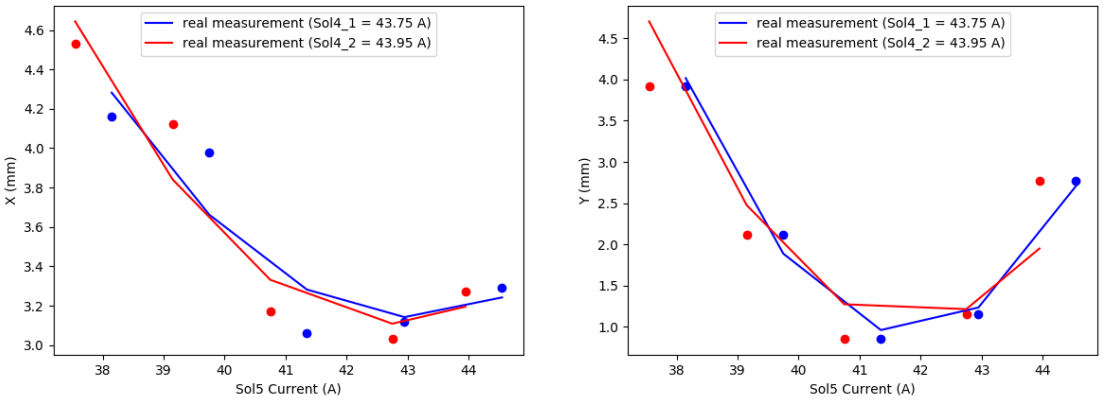

(a) (b)

Figure B.4: Plots showing the best fit of solenoid currents against the beam widths for $^{32}Si^{5+}$ beam; a) horizontal direction and b) vertical direction.

Bibliography

[1] K.L Brown And F. Rothacker *"TRANSPORT A COMPUTER PROGRAM FOR DESIGNING CHARGED PARTICLE BEAM TRANSPORT SYSTEMS"*, SLAC-91, Rev. 3 (May 1983)

[2] Helmut Wiedemann, *Particle Accelerator Physics*, *third* ed. pp. 155-158, (1999).

[3] K.T. McDonald and D.P. Russel *Joseph Henry Laboratories Princeton University, Princeton, NJ 08544*, Methods of Emittance Measurement.

[4] W.G. Davies, INTRODUCTION TO FIRST ORDER OPTICS, Two lectures given to Scanditronix Staff, May 1982,(p.27). *(Oct. 20 1988)*

[5] A. T. Green, DEVELOPMENT OF A PYTHON BASED EMITTANCE CALCULATOR AT FERMILAB SCIENCE & TECHNOLOGY (FAST) FACILITY.

[6] Z.B. Du Toit *et al* "COMMISSIONING OF THE INJECTOR CYCLOTRON FOR POLARISED AND HEAVY IONS AT NAC." *Proc.* 14^{th} *Int. Conf. on Cyclotrons and their Applications*, Cape Town, South Africa, 8-13 Oct 1995.

[7] OPERA-3d, http://operafea.com

[8] J.G de Villiers *et al* Numerical Orbit Tracking In 3D Through The Injector Cyclotron For Heavy Ions At iThemba LABS. Proc. of Cyclotrons 2016, Zurich, Switzerland.

[9] F. Nemulodi *et al* "Injection line studies for the SPC2 cyclotron at iThemba LABS" in *Proc.* 21^{th} *Int. Conf. on Cyclotrons and their Applications*, Zurich, Switzerland, 2016, p. 75.

[10] J. L. Belmont and J. L. Pabot. Study of axial injection for the Grenoble cyclotron, *IEEE Trans. Nucl. Sci., vol. 13, no. 4, pp. 191-193, 1966. doi:10.1109/TNS.1966.4324204.*

[11] A.H Bernard,*et al* Vertical focussing with a field gradient spiral inflector, 22^{nd} Int. Conf. on Cyclotron and their Applications 2019, Cape Town, South Africa.

[12] J.L Conradie *et al*, NEW DEVELOPMENTS AND A REVIEW OF THE ACCELERATOR FACILITIES AT ITHEMBA LABS. Proc. of RUPAC2012, Saint Petersburg, Russia.

[13] https://www.ucl.ac.uk/~zcapf71/Particlephysicsshow1.pdf

[14] F. Azaiez, R. Nchodu, R. Nemutudi and M. Wiedeking (2020) iThemba LABS, Nuclear Physics News, 30:4, 5-11, DOI: 10.1080/10619127.2020.1832807.

[15] https://ard.desy.de/sites2009/site_ard/content/e157650/e179572/20140822_Seidel.pdf

[16] Z.B. du Toit, Burger S.J., *et al* Aspects of the design of an 8 MeV cyclotron as injector for a 200 MeV separated-sector cyclotron, In: University of Caen, 9^{th} International Conference On Cyclotrons and their Applications, Caen, France, 7-10 September 1981. Paris : Les Editions de Physique.

[17] M. Sakildien, MSc thesis, University of the Western Cape,(2012).

[18] J.L. Conradie, PhD thesis, University of Stellenbosch, (1992).

[19] A.H Botha and Kritzinger J.J, Design of an rf system for an open-sector cyclotron, *Proc.* 7^{th} *Int. Conf. on Cyclotrons and their Applications,* Birkhäuser, Basel, p. 156-159, (1975).

[20] R.W. Thomae, *et al* Status of the new electron cyclotron resonance ion source at iThemba LABS. *Proceedings of ECRIS08, Chicago, IL USA.*

[21] The Physics and Technology of Ion Sources edited by Ian G. Brown pp.(46-48), (2004).

[22] https://shodhganga.inflibnet.ac.in/bitstream/10603/37642/12/12_chepter%202.pdf

[23] N. Angert, ION SOURCES, GSI,Darmstadt, Germany.

[24] D. Winklehner, PhD thesis, Michigan State University,(2013).

[25] https://images.app.goo.gl/SBG4giprhBjKLiMr9

[26] B. Martin, M. Grether *et al*, The Berlin 14.5 GHz ECR ion source, and its testbench for the production of slow, highly charged ions. In: University of Groningen, Proceedings of the 11^{th} internationak workshop on electron cyclotron resonance ion sources. Netherlands, 6-7 May 1993.

[27] N.Y Kheswa, PhD thesis, University of the Western Cape, (2019).

[28] J.L Conradie, J.C Cornell,& D.T Fourie, TRANSFER BEAMLINES FOR ECR AND POLARIZED-ION SOURCES FOR A NEW INJECTOR CYCLOTRON AT NAC. *Proc. of the twelfth Int. Conf. on Cyclotron and their Application*, Berlin, Germany, (1991).

[29] In Su Jung, *et al* Design of a beam buncher for the KIRAMS-30 cyclotron, (2007).

[30] B. Carlsten, Klystron Beam-Bunching lecture notes.

[31] R. Baartman and W. Kleeven, A canonical treatment of the spiral inflector for cyclotrons, (1993).

[32] Kraus-Vogt,*et al*"Emittance matching of ECR sources", Nucl. Instrum. & Meth. Vol. A268, 5(1988).

[33] Ion Beam Optics, lecture notes.

[34] F. Lohl, "Measurements of the Transverse Emittance at VUV-FE", *Diploma Thesis*. DESY-THESIS 2005-014, TESLA-FEL 2005-03, Hamburg, July 2005.

[35] Thomas P. Wangler, RF Linear Accelerators pp.(210-213), (2008).

[36] https://www.google.com/url?sa=i&source=images&cd=&ved=2ahUKEwiD85vpwv3mAhUM6RoKHUaIA_QQjRx6BAgBEAQ&

url=http%3A%2F%2Fwww.cmm.gov.mo%2Feng%2FExhibition%2Fsecondfloor%2Fmoreinfo%2F2_2_4_MagneticSuction.html&psig=AOvVaw2HpaHxCIosWW33-_KlKJYv&ust=1578899936841549

[37] Ph. Royer, Solenoidal Optics *Notes*.

[38] H. Wiedemann, *Particle Accelerator Physics.* Springer-Verlag, 2007 pp.(155-156).

[39] H. Wiedemann, Particle Accelerator Physics third edition, p.162, (2007).

[40] https://images.app.goo.gl/zJbkfu5M4Z7Lt8z28.

[41] C.M Merry Msc thesis title "CHARGED PARTICLE BEAM TRANSPORT FOR A CYCLOTRON FACILITY", University of Cape Town (1980).

[42] Dong Hyun An, Garam Hahn and Chawon Park *"Transverse Beam Emittance Measurement Using Quadrupole Variation at"* KIRAMS-430, (Received 16 December 2013, in final form 17 July 2014)

[43] Eduard Prat and Masamitsu Aiba Four-dimensional transverse beam matrix measurement using the multiple-quadrupole scan technique *Paul Scherrer Institut. CH-5232 Villigen PSI, Swirterzerland* (Received 10 July 2013; published 19 May 2014)

[44] M. Reiser *Theory and Design of Charged Particle Beams* (Wiley, New York, 1994) Chapter.4 p.199

[45] T.P. Wangler, RF *Linear Accelerators* (Wiley, New York 1998), Chapter.9 p.285

[46] K.L. Brown , A First- and Second-Order Matrix Theory for the Design of Beam Transport Systems and Charged Particle Spectrometers, SLAC-75 (June 1982).

[47] A. Wolski, "Linear beam Dynamics for Accelerators", 2012.

[48] http://cds.cern.ch/record/499098/files/p154.pdf

[49] https://www.sciencedirect.com/topics/chemistry/faradays-law

[50] J.L Conradie, *Beam Diagnostics*, Joint ICTP-IAEA Workshop on Accelerator Technologies, Basic Instruments and Analytical Techniques, 21 29 October 2019.

[51] P. Forck , Lecture Notes on Beam Instrumentation and Diagnostics, Joint University Accelerator School.

[52] P. Tenenbaum,“ Emittance Measurements in CTF 2 Drive Beam”,*CLIC Note 326,*CERN European Laboratory for Particle Physics, (1997).

[53] A.T Green Msc thesis title “DEVELOPMENT OF PYTHON BASED EMITTANCE CALCULATOR AT FERMILAB SCIENCE & TECHNOLOGY (FAST) FACILITY”, Northern Illinois University De Kalb Illinois (2016).

[54] R. Baartman, CYCLOTRON MATCHING INJECTION OPTICS OPTIMIZATION, *Proc. of PAC09, Vancouver, BC, Canada.*